Chapter 6.
Fractal and multifractal distributions.
September_17 _2016.

6.1 Introduction: Fractal geometry.

Many features of hydrothermal systems such as the spatial distribution of alteration, veining, brecciation and mineralisation are not only irregular but the same kind of irregularity is also expressed at a number of spatial scales (Figure 6.1).

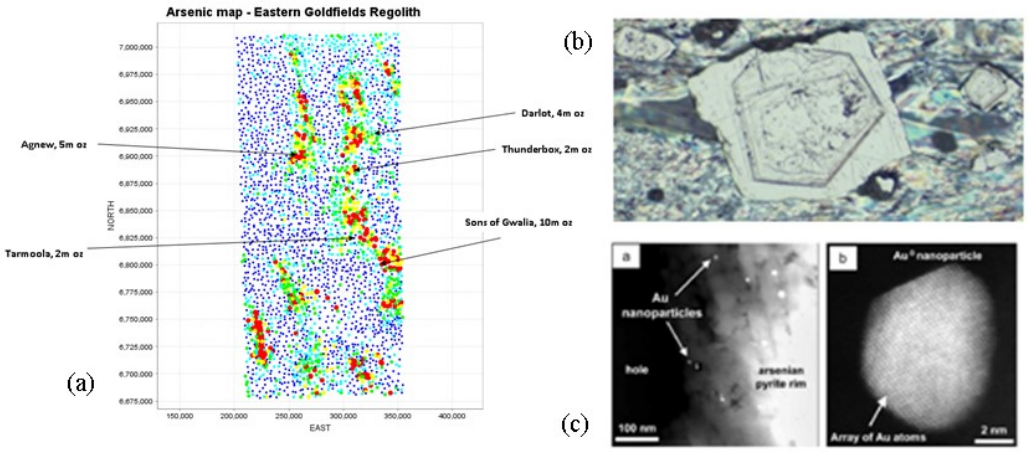

Figure 6.1. The spatial association of gold grade with arsenic expressed over 14 orders of magnitude in the Yilgarn of Western Australia. (a) Regional scale (data set supplied by Scott Halley): arsenic geochemical data set and distribution of gold mineralisation. (b) Grain-scale (Photo by Brett Davis; supplied by Scott Halley). Arsenic and gold are zoned within the pyrite. Notice similarly zoned grains of different sizes. (c)Nano-scale distribution of arsenic and gold (from Reich et al., 2005).

One way of investigating such irregularity at a wide range of spatial scales is to consider if the irregularity constitutes a *fractal geometry*. We use the term *fractal* to mean any geometrical object that has structure at all spatial scales such that when one looks at finer and finer scales one sees much the same kind of structure. We will see that for some fractals one has to homogeneously deform the small scale image (Figure 6.1 a) to statistically reproduce the large scale view of the structure. Such a fractal is called a *self-similar* fractal. Formally a *fractal is an object that has structure at all length scales and some measure of this structure is invariant with respect to an affine transformation* (Mandelbrot, 1982). This means that the object has structure within structure. From a mathematical point of view the way in which the structure scales with length is a power law:

$$P(\varepsilon) \approx \varepsilon^{D} \qquad (6.1)$$

where $P(\varepsilon)$ is the probability that a part of the object lies within a box of size ε (examples are the presence of fractures or of gold within a box of size, ε); ε is a length scale and D is commonly known as the *fractal dimension*.

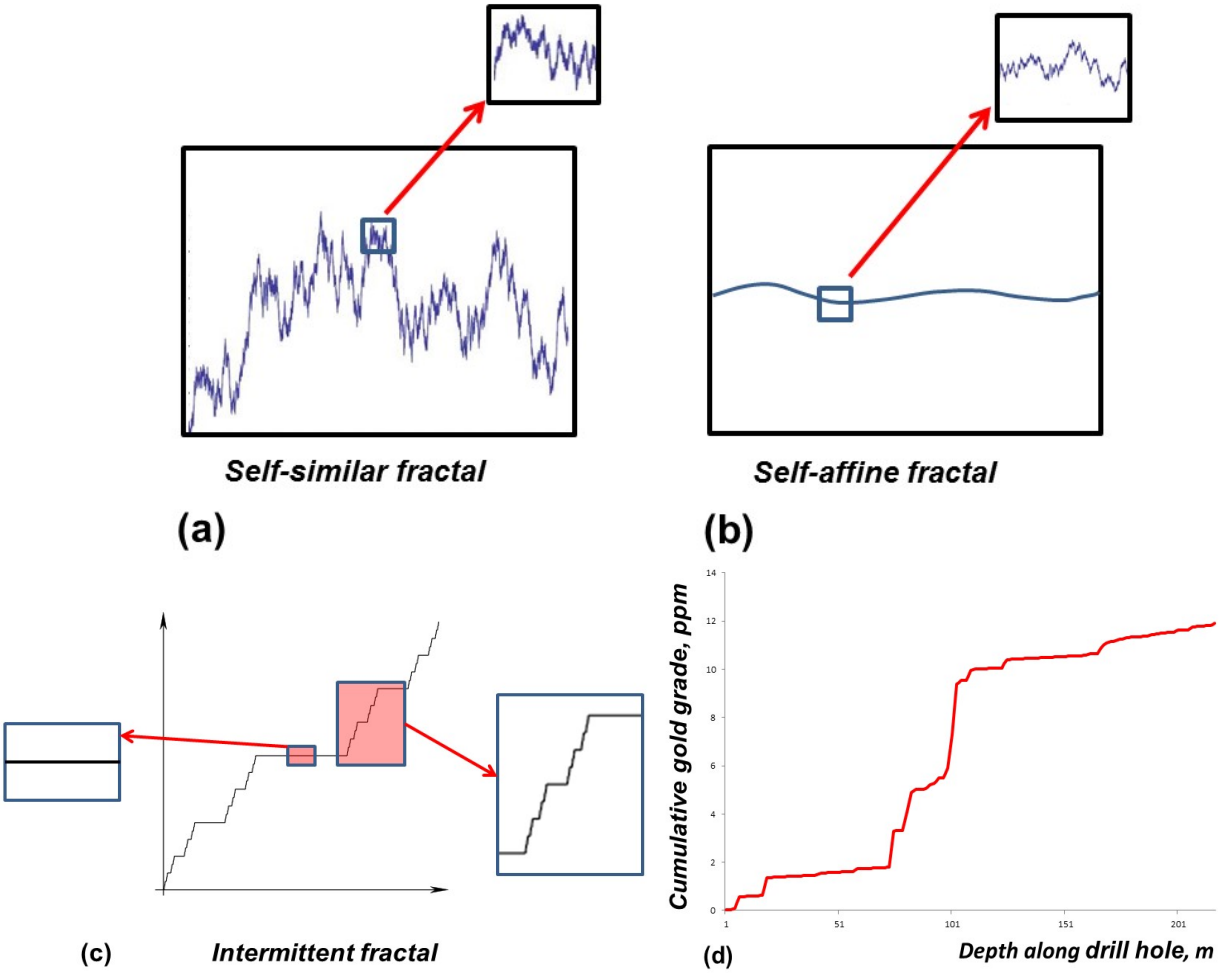

Figure 6.2. Some classes of fractals. (a) Self-similar fractal. (b) Self-affine fractal. (c) Intermittent fractal. (d) An intermittent fractal expressed as the cumulative gold grade along a 200 m diamond drill hole from Sunrise Dam mine, Western Australia.

It is important in what follows to distinguish between simply noting whether some part of the object lies within a box of given size as opposed to noting the concentration or some *measure* of the object within that box. An example is to note whether gold exists within a given box as opposed to noting the concentration of gold within that box. The first way of representing the image leads to the determination of the *fractal dimension* whereas noting the concentration or measure within each box leads to a determination of the *multifractal spectrum* (if it exists). In mathematical terms, a fractal is a *set* (or array of objects) whereas a multifractal can arise if one assigns values (or a *measure*) to each point in the set.

It should be appreciated that not all fractals are self-similar. *Self-similar fractals* remain the same under the influence of any transformation that is a *dilation* (a contraction or expansion of equal magnitude in all directions (Figure 6.2 a). The word *same* here is meant to imply that at different scales the pattern has identical statistical properties as measured say by the probability distribution (see Frisch, 1995, his Chapters 3 and 8). Fractals also exist that are *self-affine* (Figure 6.2 b); these are objects that remain the same under *affine transformations* (for instance, a homogeneous biaxial distortion) other than a dilation. Thus a surface such as a fault plane appears smooth at a coarse length scale but is rough at a fine length scale. These surfaces

are *self-affine fractals*. Scale invariance cannot continue indefinitely and so fractal geometries are practically restricted in hydrothermal systems to three to perhaps five or six orders of magnitude in length scales (corresponding say to scaling from 1mm to 100 m or 1 km). There are other types of fractals, a common one in hydrothermal systems being an *intermittent fractal* (Figure 6.2 c). Here magnification of different parts of the fractal gives different results in that intermittent fractals show fractal behaviour for some parts of the system but not for others. Gold distributions are classical examples of intermittent fractals (Figure 6.2 d).

Fractals are *singular*[1] *functions* from a mathematical point of view since they cannot be differentiated and so D is also known as a *singularity measure*. The interesting feature of (6.1) is that D is commonly a non-integer. As we saw in Chapter 5, the reason that self-similar geometries follow a power law of the form (6.1) is that it is the only form of relation where changing the size of ε leaves the form of the equation unaltered. Thus if we double the size of ε we get

$$P(\varepsilon) \approx (2\varepsilon)^D = 2^D \varepsilon^D \qquad (6.2)$$

which is of the same form as (6.1).

The method for determining D in (6.1) consists of placing an array of boxes (or balls) of size ε on the space occupied by the object and counting the proportion of boxes, $P(\varepsilon) = N(\varepsilon)/N$, that contain part of the object (Figure 6.3 a). This is repeated for different values of ε (Figure 6.3 b) until the proportion of boxes that cover the object at a range of length scales is established; here N is the total number of boxes of size, ε, that cover the object. After a large number of iterations of this process one plots the logarithm of the proportion of boxes for a given ε that contain parts of the object against the logarithm of ε. If the object is a fractal (or to be precise, follows a power law) then this plot is a straight line with slope $-D$ (Feder, 1988; Schroeder, 1991). That is, the relation is of the form (6.1), where $P(\varepsilon)$ is now the proportion of boxes of size ε that contain part of the object. This process is called *box counting* and descriptions of the process with applications to structural geology are given in Kruhl (1994). Applications to mineral systems are given by Arias et al. (2011), Bastrakov et al. (2007), Hunt et al. (2007), Li et al. (2009), Oreskes and Einaudi (1990), Qingfei et al., (2008), Riedi (1998) and Sanderson et al. (2008). Fractal (or at least, power law) distributions of mineralisation are reported by Carlson (1991), Schodde and Hronsky (2006) and Ford and Blenkinsop (2009). D is commonly known as the *box counting dimension*.

[1] Mathematically, a singularity is some behaviour of a function that cannot be defined mathematically. This may mean, for instance, that the function is discontinuous, diverges to infinity or that it is not differentiable at a particular point.

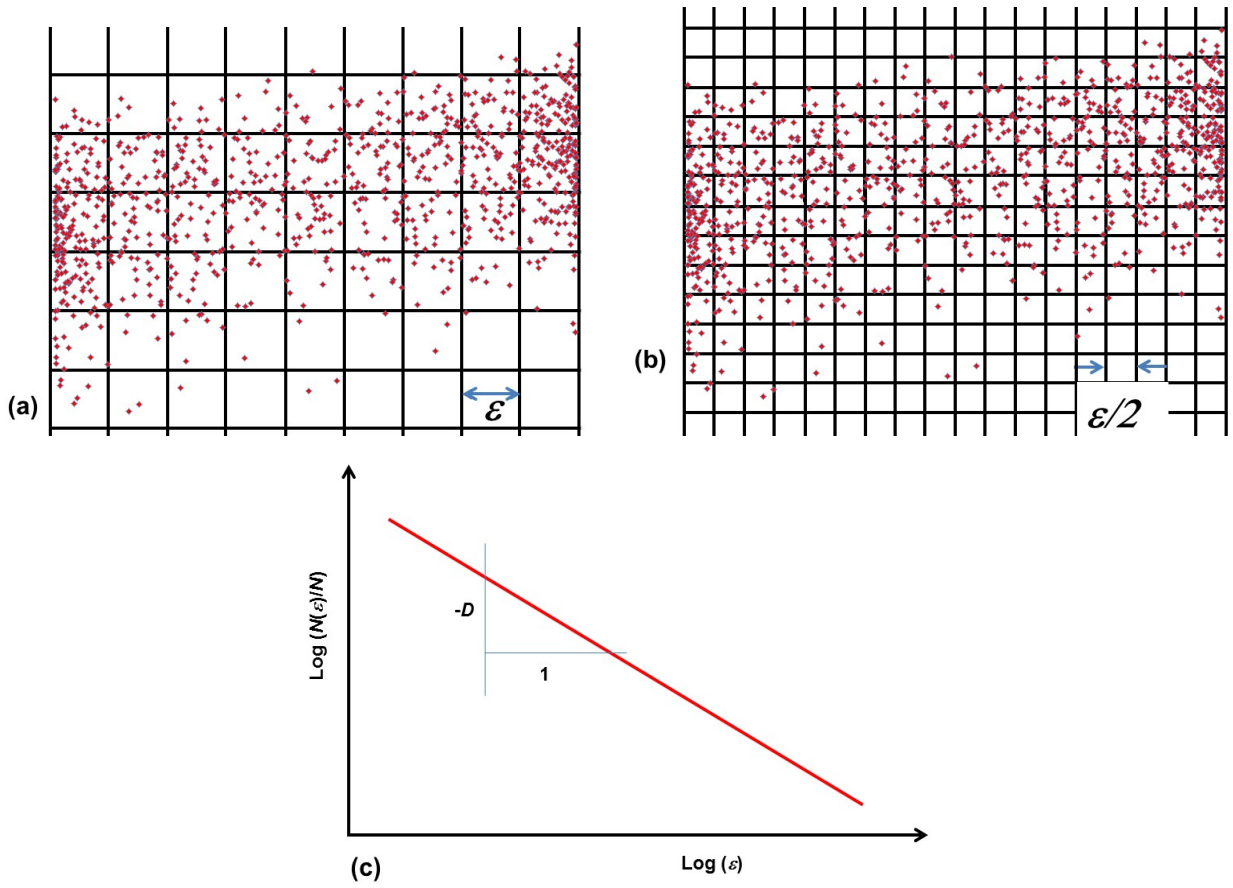

Figure 6.3. The box counting method of establishing the fractal dimension. (a) A grid with grid-size ε is laid over the image and the proportion, $N(\varepsilon)/N$ of grid squares that contains at least one point is recorded. N is the total number of squares in this case that covers the object. (b) The process is repeated with the grid size changed (in this case to $\varepsilon/2$). (c) A log-log plot of $N(\varepsilon)/N$ against ε gives the box counting fractal dimension, D.

One should be aware of the pitfalls involved in fitting power laws to measured data sets and that a power law distribution established over a limited range of length scales does not necessarily imply a fractal geometry; this can be the situation, for instance, if the probability distribution is log-normal (Figure 6.4; see discussion by Sornette, 2006, pp 94 - 96). This last limitation is important since all hydrothermal systems have a limited size. For a detailed discussion of power laws see Newmann (2006).

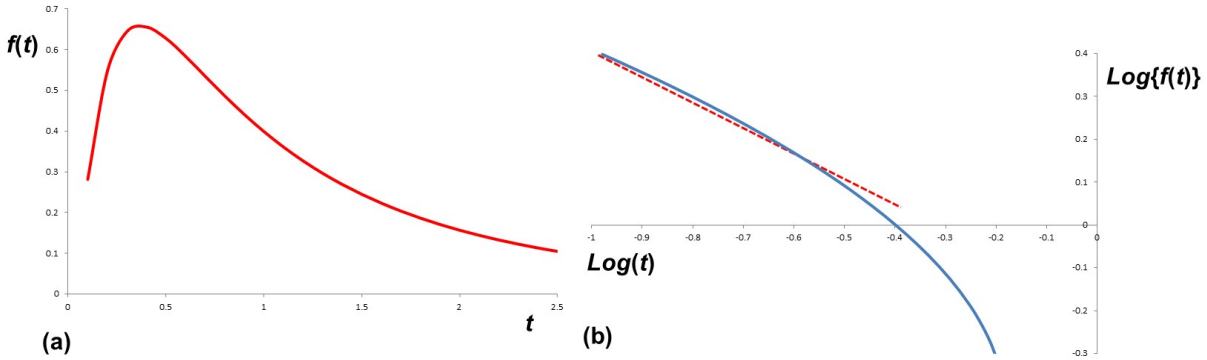

Figure 6.4. A log-normal distribution. (a) Density function for a log-normal distribution given by $f(t) = \frac{1}{t\sigma_L\sqrt{2\pi}} \exp\left[-\frac{\left(ln(t) - \mu_L\right)^2}{2\sigma_L^2} \right]$ with $\mu_L = 0$ and $\sigma_L = 1.0$. (b) A plot of $log\{f(t)\}$ against $log(t)$ for part of the distribution in (a). Notice the approximate linear fit over a limited range of $log(t)$.

Other dimensions of use in describing fractal geometries are:

- *The information dimension* which is related to the sum of the probabilities, p_k, of finding a part of the object in the k^{th} box of size ε:

$$D^{information} = \lim_{\varepsilon \to 0} \frac{-\sum_k p_k \log p_k}{\log \varepsilon} \qquad (6.3)$$

and

- *the correlation dimension* which is a measure of the number of pairs of points whose distance apart is less than r:

$$D^{correlation} = \lim_{r \to 0} \frac{-\sum_k \log C(r)}{\log r} \text{ where } C(r) = \frac{1}{N^2} \sum_{i \neq j} \mathcal{H}\left[r - \left| x_i - x_j \right| \right] \qquad (6.4)$$

where $\mathcal{H}$ is the Heaviside function: $\mathcal{H}(x) = 0$ for $x \leq 0$ and $\mathcal{H}(x) = 1$ for $x > 0$. $C(r)$ is known as the *correlation sum*. We will see that both these dimensions have special meanings within a multifractal spectrum but for a monofractal, $D = D^{information} = D^{correlation}$.

6.2. Multifractal measures.

The geometry of hydrothermal fabrics is more complicated than being characterised by a single value of D as we will see below. If the measure of an object is characterised by a single value of D then it is called a *monofractal*. Some measures are characterised by two values of D and these are called *bifractals*. However if the geometry is characterised by many different values of D at different points then the measure is clearly more complicated and is called a *multifractal* (Mandelbrot, 1974); a spectrum of D values arises. A multifractal therefore consists of a set of interwoven fractal measures and is characterised by a spectrum of singularity measures. An example consists of a precipitation process, for say gold, that is itself fractal but is controlled spatially by a fractal distribution of the pore or fracture space within which precipitation occurs. The spatial distribution of gold concentration is then multifractal. For reviews of the development of the multifractal concept see Feder (1988), Bohr and Tel (1988), Beck and Schlögl (1993), Arneodo et al. (1995), Schroeder (1996), and Sornette (2006).

Another way of thinking of irregular *measures* is in terms of homogeneity and heterogeneity. Fractal measures may be homogeneous in the sense that every part of the geometry is characterised by a single value of D in (6.1). Such geometry is called a *monofractal* geometry. However most fractal measures are heterogeneous in the sense that different parts of the geometry are characterised by different values of D. These geometries are called *multifractal* geometries. Commonly in heterogeneous fractals, fractal sets with different values of D are intertwined at a fine scale (Figure 6.5) and are difficult to analyse except by employing analytical techniques that can zoom into the fine scale. We will see in Chapter 9 that *wavelet transforms* are one way of doing this.

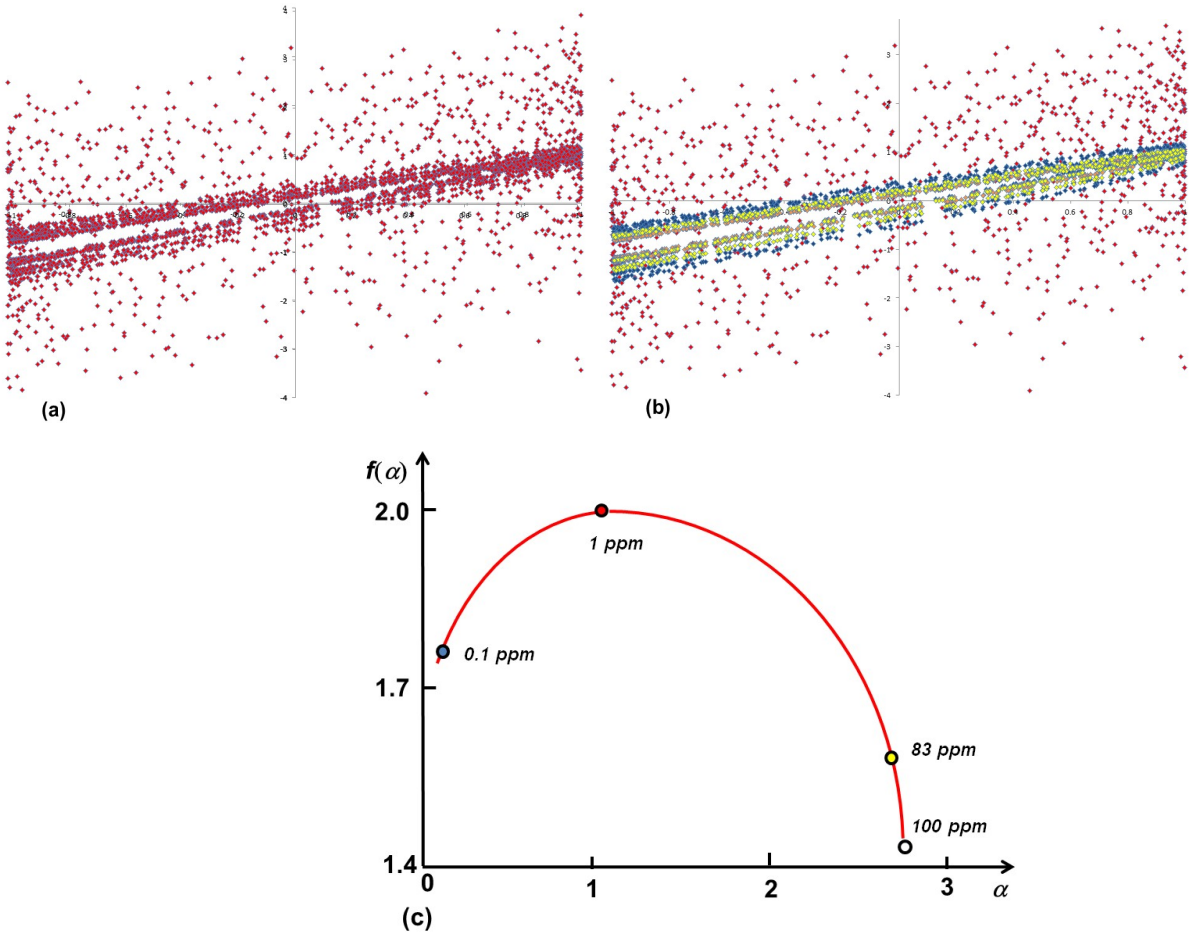

Figure 6.5. A multifractal geometry. (a) This image consists of four monofractals, produced by the Kaplan-Yorke Map, (5.5), embedded in each other. (b) Delineation of the four monofractals in (a) with D = 1.43 (whiteSSS), D = 1.58 (yellow), D = 1.76 (blue) and D = 2 (red). (c) Multifractal singularity spectrum arising from (b) where gold grades have been defined on the set described by (a) as a measure.

In Figure 6.5 the principles behind the development of a *multifractal* and its associated *singularity spectrum* are illustrated. In Figure 6.5 (a) some of the attarctors for the Kaplan-Yorke Map, (5.5), are plotted for the values of λ in (5.5) of 0.2, 0.3, 0.4 and 0.9. The attractors are not differentiated and points from each attractor are given the same colour. Figure 6.5 (a) constitutes a *set* which is a fractal with fractal dimension (D = 2) the same as that of the sparcest attractor corresponding to λ = 0.9. In Figure 6.5 (b) the four attractors in (a) are delineated by colour: white for λ = 0.2 (D = 1.43), yellow for λ = 0.3 (D = 1.58), blue for λ = 0.4 (D = 1.76) and red for λ = 0.9 (D = 2.0). These fractal dimensions are calculated from the discussion of the Kaplan-Yorke Map in Chapter 5. We now associate, as an example, a gold grade with each colour: white: 100 ppm by weight; yellow: 83 ppm; red: 1 ppm and blue: 10^{-1} ppm. Figure 6.5 (b) now constitutes a measure, which we call μ, representing the distribution of gold grade, superimposed on the fractal set defined by Figure 6.5 (a). The set shown in Figure 6.5 (a) is known as *the support for the measure.* We now define a quantity α, known as the *singularity strength*, by the relation:

$$\alpha = \lim_{\varepsilon \to 0} \frac{\ln \mu}{\ln \varepsilon} \qquad (6.5)$$

and instead of proceeding to the limit we select a small value for ε of say 10^{-6} . α now takes on the values given in Table 6.1.

Table 6.1. Quantities used to construct the singularity spectrum, Figure 6.5 (c).

Gold grade, μ, ppm by weight	Colour in Figure 7(b)	Probability of occurrence, P_μ	$\alpha \simeq \frac{\mu \ln P_\mu}{\ln(10^{-1})}$	$f(\alpha) \equiv D_{local}$
100	White	10^{-3}	2.7	1.43
83	Yellow	20.8×10^{-3}	2.67	1.58
1	Red	0.01	1.0	2.00
0.1	Blue	0.1	0.1	1.76

Since $0 \le \mu \le 1$, *and* $\ln \varepsilon \to$ *a large negative number as* $\varepsilon \to 0$, α *is always positive and is* proportional to the natural logarithm of the gold concentration. $f(\alpha)$ is plotted against α in Figure 6.5 (c). A $\bigcap$–shaped curve is produced which is typical of many multifractal distributions. However, as one can see from Figure 6.5 (c), a precise $\bigcap$–shaped curve demands quite precise processes that generate a closely coupled relationship between $f(\alpha)$ and α. Such precision (if demonstrated) is surely an important imprint of coupled processes that is worthy of further investigation.

The precise shape of the $\bigcap$– curve is quite sensitive to the ways in which the range of the measure and the ways in which the monofractals representing each value of the measure are distributed in space. If, for instance, all of the high gold grades are distributed over a wide range of fractal dimensions, from sparse to space filling, whilst the low grades have a restricted range of fractal dimensions, the $\bigcap$– shape is skewed to the left. If all low grades have much the same fractal dimension expressed as distributions that a space filling the singularity spectrum may be "one-sided" (Mandelbrot, 19xx): $\sqcap$. If the highest and lowest grades are similar then the arms of the $\cap$ are close together. If the highest and lowest grades are far apart the $\bigcap$– shape is relatively open.

As we saw in Chapter 1, a hydrothermal system is part of a lithospheric scale energy cascade whereby the deformation and fluid/heat flow within an element of the lithosphere is controlled at the largest of scales by the velocity boundary conditions imposed by the large scale tectonic regime together with pressures (arising from the dead load exerted by the overlying rock mass and other contributions generated by topographic relief) and temperature changes arising from the impingement of heat sources and/or advection of the element through the geothermal gradient of the Earth. Such advection also contributes to changes in the pressure. Thus at the coarse scale a deformation gradient drives momentum transfer whilst changes in temperature and pressure (both solid and fluid pressures) induce changes in chemical potentials that drive mineral

reactions. In this process, forcing at lithospheric scales drives a cascade of dissipation at finer and finer scales within the lithosphere until at a very fine scale the dissipation is negligible. The development of lithospheric scale buckles and fault systems is part of a dynamical cascading process whereby structure is developed at finer and finer scales. At the coarse scale dissipation is dominated by deformation coupled with heat diffusion; at finer scales heat diffusion ceases to be dominant as a dissipative mechanism and the dissipative processes are dominated by local deformations, exothermal mineral metamorphic mineral reactions (alteration) and structural rearrangements such as fracturing, veining and brecciation. Finally energy is stored in endothermic mineral reactions (precipitation of sulphides, metals such as gold and anhydrous silicates such as quartz). Such a cascading process is similar to that proposed for fluid turbulence (Chapter 1) where large eddies break down to shed eddies at smaller and smaller scales (Richardson, 1922; Drazin and Reid, 1981; Frisch, 1995; Kestner and Arneodo, 2003).

These cascading processes lead to multifractal geometries and so it is of importance to develop efficient ways of measuring and characterising the scaling properties of structures in deformed, altered and mineralised rocks since there is the potential that such properties reflect the details of the cascading process. In Chapter 9 we discuss the *wavelet transform* method as a means of achieving this characterisation.

Why should a cascade process produce multifractal geometries? The answer lies in different processes operating at different length and time scales (and hence obeying different scaling laws) to produce the same feature. We offer two examples below.

(i) Precipitation of gold:

The scale dependence of the processes involved in the generation of a hydrothermal gold deposit is illustrated below:

- At the scale of 10^3 m the gold deposition process involves focussed flow in three dimensional fracture networks where the geometry of these networks promotes chaotic mixing (Chapter 7 and Lester et al., 2011, 2012). The flow rates may be such that laminar flow is ubiquitous at each instant but the network geometry promotes chaotic flow (Chapter 7). Or, the flow rates may be higher so that the flow is turbulent. Either way chemical reaction rates are enhanced by the chaotic flow.
- At the scale of 10^2 m the flow may be in breccia and vein networks where again the three dimensional geometry promotes chaotic mixing. Since the Reynolds number is smaller than at the 10^3 m scale the dependence on scale is different for the two cases.
- At the 1 m scale gold deposition is by a reaction-transport process with reactions at the boundaries of flow induced chemical heterogeneities.
- At the scale of 10^{-3} m reaction-diffusion-transport reactions at grain interfaces dominate with the scale of precipitation controlled by fluctuations in fluid concentration of multi-valence elements such as As that can contribute an electron to the reaction:

$$\mathrm{Au}^{+}_{(fluid)} + e^{-} \rightarrow \mathrm{Au}_{(solid)}$$

- At the scale of 10^{-6} m solid state reaction-diffusion reactions at chemical potential contrasts (such as gradients in arsenic concentration) precipitate nano-scale gold whose spatial distribution is controlled by diffusion.

(ii) Development of fracture systems:

The scale dependence of the processes involved in fracture formation is illustrated below:

- At the scale of 10^3 m fracture propagation may be faster than fluid diffusion in the porous host rock mass so that fracture propagation is driven solely by stresses at the crack tip. The scale of fracturing is related to the stress diffusivity.
- At the scale of 10^2 m the velocity of crack propagation is limited by the diffusion of fluids to the crack tip thus promoting local hydrofracture. The spacing is controlled by the competition between stress and fluid diffusivities.
- At the scale of 1 m crack propagation is controlled by stress corrosion at the crack tip. Spacing of fractures is controlled by the rate of transport of stress corrosion materials to the crack tip.
- At the sale of 10^{-3} m crack spacing is controlled by competition between supply of fluid to the crack tip and healing of the crack by precipitation in the crack.

In Chapter 5 we saw examples of how fractal structures develop in a system as a means of minimising the energy of the system. In general such processes involve an iterative procedure of some kind whereby the system continuously branches in a self-similar manner to produce replicas on a finer and finer scale. Such iterative processes are a mechanism of producing self-similar structures at a finer and finer scale and the *Iterative Function System* (IFS) of Barnsley (1988) is one way of expressing such a process. Other ways of producing fractal structures involve escape functions and random walk processes (Feder, 1988; Schroeder, 1991). The development of percolation networks during flow in porous media is an example of a random walk process (Arneodo et al., 1995). In Chapter 9 we will consider some iterative processes that have been proposed to develop multifractal distributions of mineralisation in hydrothermal systems.

6.3. Probability distributions.

It is useful to classify systems so long as the classification is not simply "stamp collecting". Any useful classification should emphasise the basic physical and chemical nature of the system and/or point to the tools needed to analyse the system in terms of the physical and chemical processes responsible for the development of the system. We have seen in Chapter 5 that systems can be usefully classified according to whether they are:

- Deterministic or stochastic.
- Complicated or complex.
- Critical or non-critical.
- Homogeneous or heterogeneous.

Another classification of nonlinear systems, is:

- Non-fractal or fractal; *in particular if a system is fractal, is the distribution of some measure of the structure, mono-fractal, or multifractal*?

The geometry of some spatial distribution, μ, can be classified according to the probability distribution displayed by μ. Such distributions can be of two types:

- Statistically homogeneous distributions; such distributions display fast decaying or "light" tails such as are typical of Gaussian or Poisson distributions (Figures 6.6 a, b). These kinds of distributions are typical of geometries far removed from critical states.
- Statistically heterogeneous distributions; such distributions have skewed or "heavy" tails and scale independent spatial distributions of μ (Figures 6.6 c, d). These kinds of distributions are power-law distributions typical of fractal geometries developed in systems that are at criticality.

As one approaches criticality there is commonly a continuous progression from homogeneous, fast decaying distributions to heterogeneous, scale independent distributions at criticality (Figures 6.6 e, f, g). Girard et al, (2010) have analysed the distribution of deformation intensity and of energy release in a simulation of a deforming elastic-plastic material approaching peak load and have shown that the distribution of deformation displayed in Figure 6.6 (e) is in fact multifractal.

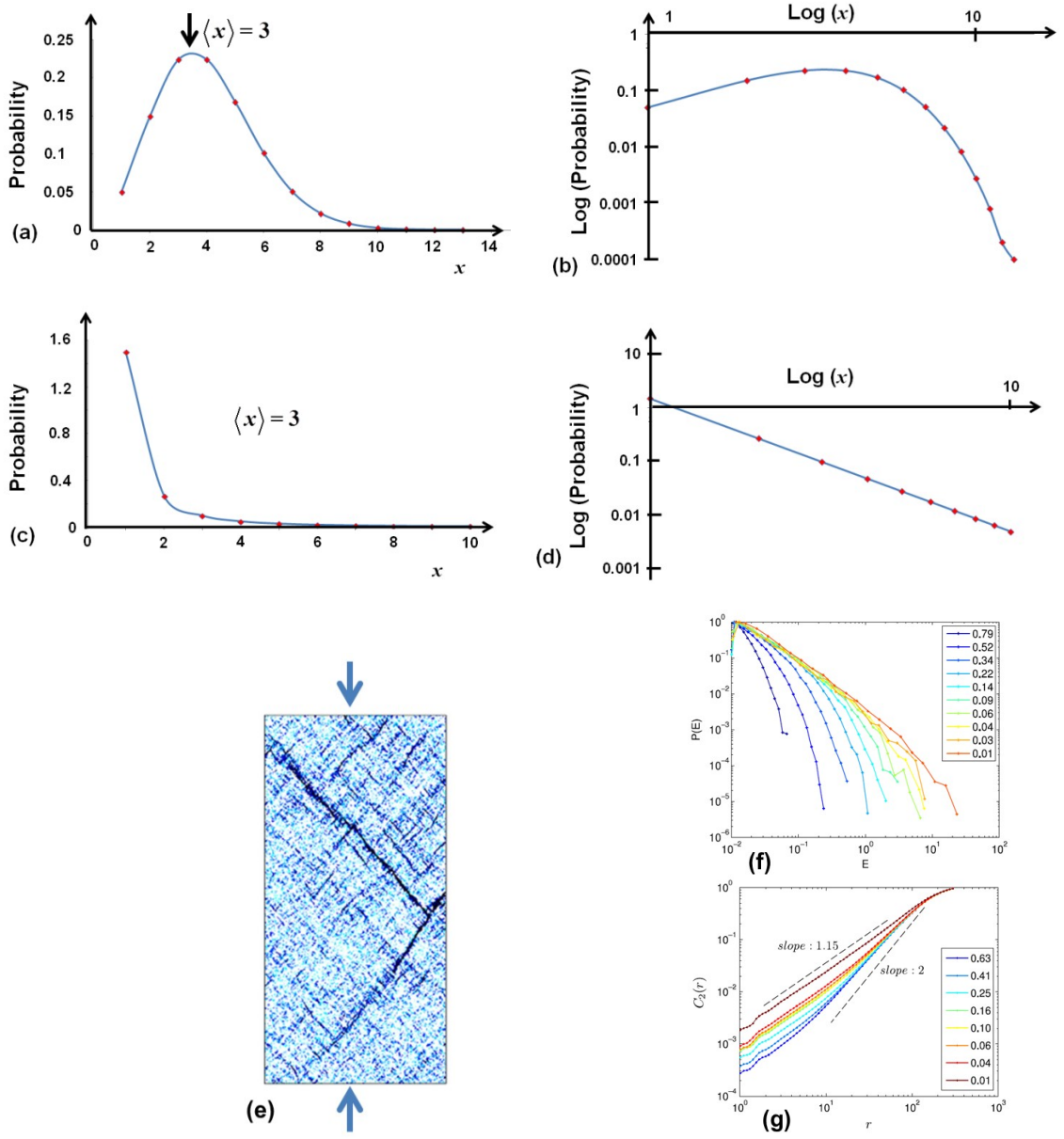

Figure 6.6. Homogeneous and heterogeneous probability distributions. (a) Poisson distribution (an example of a "light" tailed distribution) with a mean of $\langle x \rangle = 3$. (b) Log(probability) versus log(x) corresponding to (a) showing rapid decay of the probability with increasing x. (c) A power-law probability distribution (a "heavy" tailed distribution) with a mean of $\langle x \rangle = 3$. (d) Log(probability) versus log(x) corresponding to (c) showing scale invariance of the probability with increasing x. (e) Numerical simulation of an elastic-plastic material showing the spatial distribution of localised deformation. From Girard et al. (2010). (f) Probability distribution, P(E), of the magnitude of dissipated energy, E, normalised by its maximum value, associated with deformation avalanches in (e) for departures, Δ, from peak load shown by different colours. A small value of Δ indicates that the specimen is close to peak load. (g) Variation of the correlation integral, $C_2(r)$ with distance, r, from an event in (e) for departures, Δ, from peak load shown by different colours. A small value of Δ indicates that the specimen is close to peak load. A slope of 2 indicates a homogeneous distribution of deformation whereas a slope of 1.15 indicates the system has developed a spatial distribution of deformation that is scale invariant. That is, the system is critical.

Notice that close to criticality the probability distributions shown in Figure 6.6 (f) follow the fractal distribution corresponding to criticality but drop off as E increases. This could be interpreted as two different fractal distributions. The probability distribution then resembles the "bifractal" spatial distributions of gold mineralisation reported from Zambezi (Ford and Blenkinsop (2009) and Nevada (Carlson, 1991). We interpret these " bifractal" distributions as an indication that the plumbing systems for these well endowed areas are sub-critical (see Chapters 3 and 5).

6.3.1 Correlations: The Hurst exponent.

Consider a one dimensional sequence of values, $\xi(d)$ representing the concentration of a particular mineral phase or the degree of fracturing or some other quantitative measure of the fabric of a hydrothermal system. In the example we take, ξ varies with distance, d, as shown in figure 6.7. We can characterise the resulting pattern in a number of ways. One way is to use the *Hurst exponent* (Feder, 1988; Sprott, 2003) which measures the way in which the local range in variation (or roughness) scales with distance across the structure. In order to calculate the Hurst exponent we first take the mean of ξ and then (figure 6.7) the cumulative departures from the mean, $\Xi(d)$. If R is the *range* of Ξ, that is, the difference between the largest and smallest value of Ξ, then the Hurst exponent, H, is defined by:

$$\frac{R(d)}{\sigma(d)} = \left(\frac{d}{2}\right)^H$$

where $\sigma(d)$ is the standard deviation of ξ over the distance d. Examples of signals with different Hurst exponents are given in Figure 6.8 (a) and characteristics of signals for various values of the Hurst exponent are given in Table 6.1. Figure 6.8 (b) compares white noise, monofractal and multifractal signals.

Table 6.1. Characteristics of the Hurst exponent, H, for a one dimensional signal.

Value of H	Meaning	Pattern characteristics
$0.5 < H < 1$ Persistent	Long range positive autocorrelations	A high (low) value tends to be followed by another high (low) value. The overall trend is to higher (lower) values. Power law decay in autocorrelations.
$H = 0.5$	Completely uncorrelated sequence.	Autocorrelations at small intervals can be positive or negative. Absolute value of autocorrelations decays rapidly to zero.
$0 < H < 0.5$ Antipersistent	Long range switching between high and low values	A high value tends to be followed by a low value. Power law decay in autocorrelations.

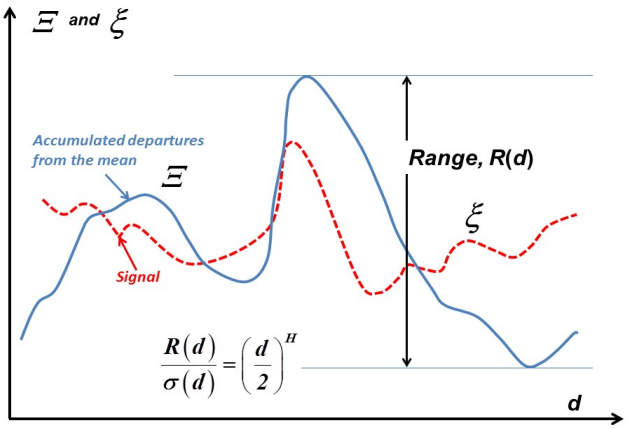

Figure 6.7. Definition of the Hurst exponent, H. ξ is the initial data as a function of distance, d, and Ξ is derived from these data as the cumulative departure of the data from the mean. R is the range of Ξ, that is the difference between the maximum and minimum value of Ξ. If σ is the standard deviation of ξ then the Hurst exponent is defined by $\frac{R}{\sigma} = \left(\frac{d}{2}\right)^H$.

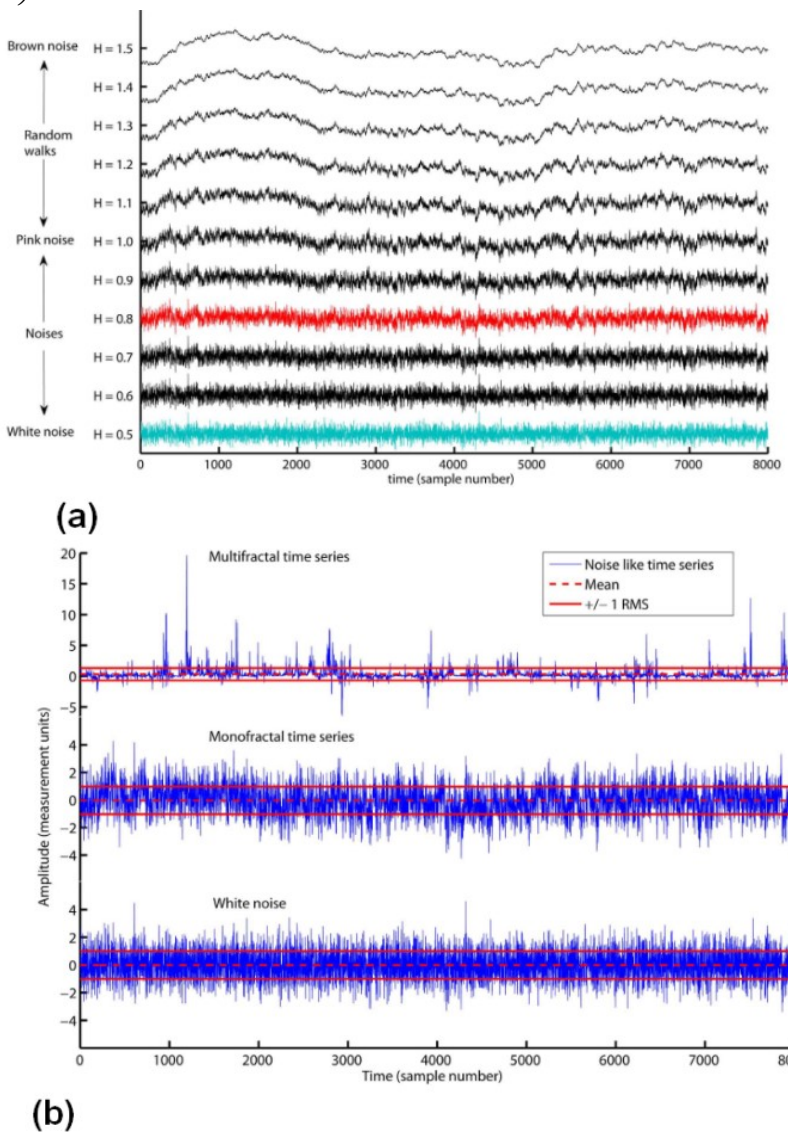

Figure 6.8. Comparisons of different types of signals. (a) Signals for Hurst exponents ranging from 0.5 to 1.5. (b) Comparison of white noise with monofractal and mutifractal signals. The ± RMS range for each signal is about the same but notice the change of scale for the multifractal signal.

6.4. Some useful features of systems characterised by fractal and multifractal distributions.

In this section we first (Section 6.4.1) consider a useful technique that enables us to analyse some fractal geometries that arise from nonlinear dynamical systems. This involves the construction of *delay maps* that reproduce the phase diagrams of dynamical systems even though the underlying mathematical equations or physical/chemical processes are unknown. Delay maps are important for characterising chaotic signals and for testing models that are proposed to explain the signals. We then proceed (Section 6.4.2) to discuss some aspects of probability theory of use in interpreting fractals and multifractals.

6.4.1 Delay maps.

It turns out that a further useful classification concerns the probability distributions that various data sets associated with the system take on. Most linear systems produce observable responses that can be represented by simple mathematical expressions such as straight lines, periodic functions (Figure 6.9 a), quasi-periodic[2] functions (Figure 6.9 c) or combinations of such functions. Combinations of functions are possible because linear functions obey the mathematical law of superposition which says that if the governing equations for the system have solutions X and Y then a linear combination of these two solutions aX + bY, is also a solution where a and b are (rational or irrational) numbers.

However, combinations of many strictly periodic or quasi-periodic functions can generate quite complicated signals (Figure 6.9 a and c) some of which may resemble chaotic signals (Figure 6.9 e). It is useful to have a technique that distinguishes such alternatives and at the same time gives some insight into the underlying processes that produced the signal. The commonly used technique is that of Fourier analysis (Bloch, 2003) that breaks the signal into its component (periodic) parts. In Figures 6.9 (b and d) the Fourier transform of the signals in Figures 6.9 (a and c) are shown. The individual wavelengths that make up the signal are easily delineated. This procedure works exceptionally well for combinations of strictly periodic and quasiperiodic signals but for chaotic signals the outcome is identification of "noise" (Figures 6.9 e and f).

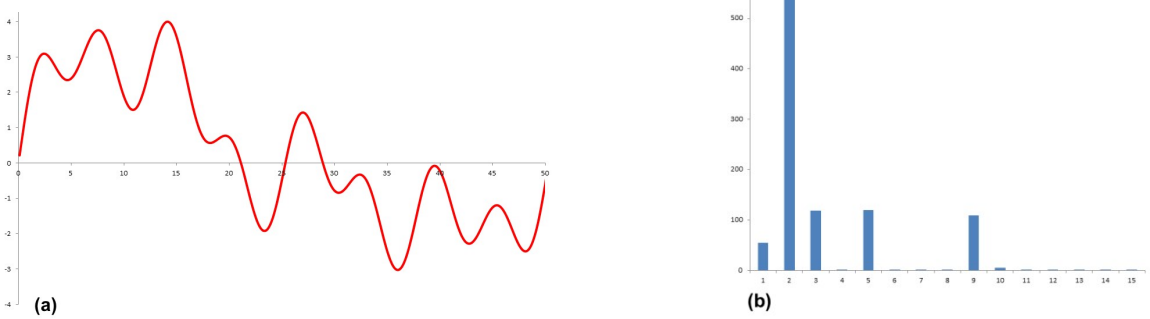

[2] A quasi-periodic function is one that is almost periodic but never repeats itself. An example is the function: $y = A\sin(\alpha x) + B\sin(\beta x)$ where the ratio α/β is an irrational number such as π, 1/6 or $\sqrt{2}$.

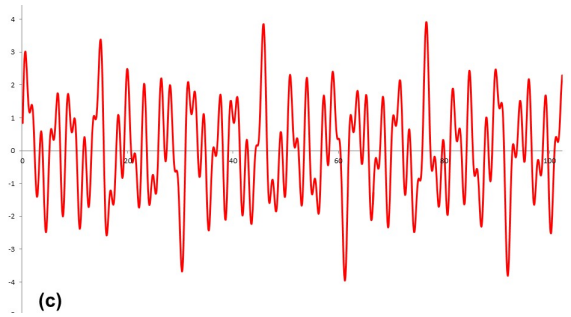

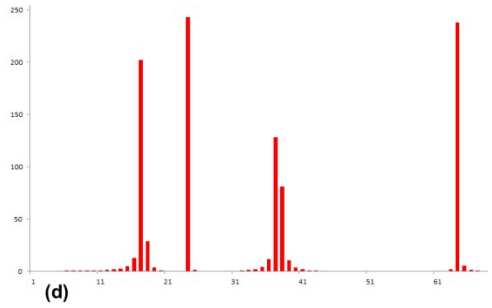

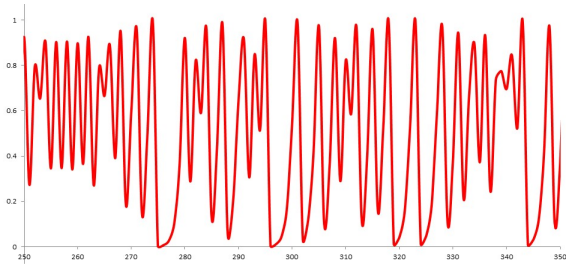

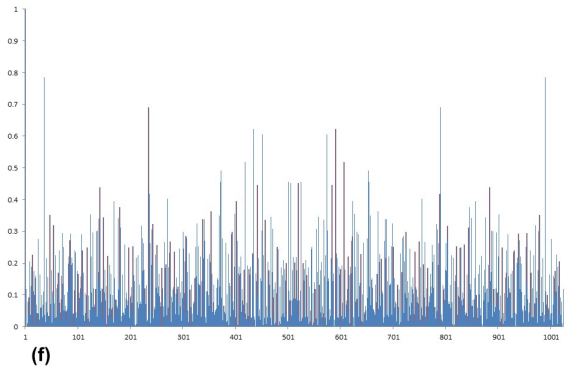

Figure 6.9. Various signals and the corresponding Fourier analyses. (a) The signal y=sin(x)+sin(x/2)+sin(x/4)+sin(x/6)+sin(x/8))+sin(x/10). (b) The corresponding Fourier analysis. (c) The signal $y = \sin(x) + \sin(\sqrt{2}x) + \sin(\sqrt{5}x) + \sin(\sqrt{15}x)$. (d) The corresponding Fourier analysis. (e) Signal resulting from the logistic map: $x_{n+1} = 4x_n\left(1 - x_n\right)$ for iterations 250 to 350. (f) The corresponding Fourier analysis for the first 1024 iterations. All figures calculated using an EXCEL spread-sheet (see Bloch, 2003 for details of Fourier transforms using EXCEL).

A far more elegant technique of relevance to chaotic data sets is that of a *delay map* (Packard et al., 1980; Takens, 1980, and Crutchfield et al., 1986) whose basis can be seen most clearly by considering the simple logistic equation we investigated in Chapter 5 and is illustrated in Figures 6.8 (e and f). One version of this map is given by

$$x_{n+1} = 3.8x_n\left(1 - x_n\right) \qquad (6.6)$$

In Figure 1.13 we saw that, with the use if an EXCEL spreadsheet and starting with x_n = 0.1 we can readily calculate an array of values for x_{n+1} and x_n. We plot x_{n+1} against x_n in Figure 6.10. The result is a plot of the function (6.6). This is the basis of all delay maps. Some further examples are given in Figures 6.11 and 6.12.

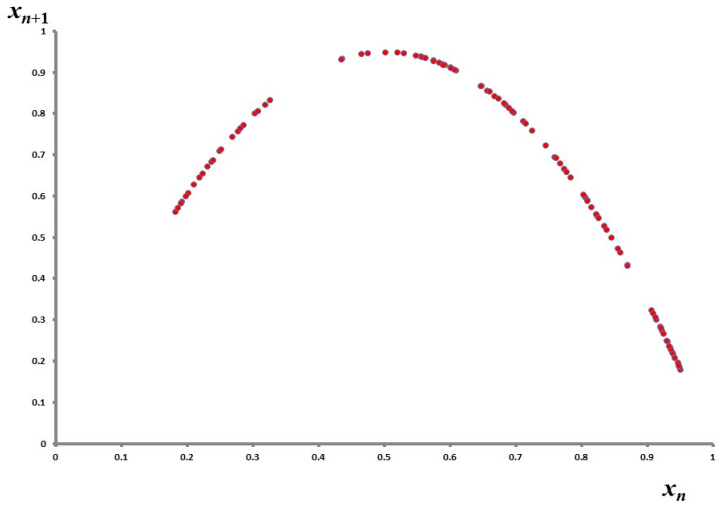

Figure 6.11. The delay map for the logistic map: $x_{n+1} = 3.8x_n\left(1-x_n\right)$. The first 100 iterations are plotted.

In Figure 6.11 (a) a simple sine curve is plotted given by $y_n = \sin\left(x_n\right)$ whilst in Figure 6.11 (b) y_n is plotted against y_{n+N} for N =1 (blue curve) and for N =16 (red curve). Both produce closed ellipses with the aspect ratio of the ellipse decreasing as the value of N corresponding to the period of the signal is approached. Figure 6.11 (b) is a delay map for the sine-wave signal in Figure 6.10 (a). A similar plot is shown in Figure 6.11 (d) corresponding to the quasi-periodic plot in Figure 6.11 (c). The delay map now consists of a series of nested elliptical spirals that never repeat themselves; however the signal is not chaotic since one can confirm that there is no sensitivity to initial conditions. Nonlinear systems as we have seen in previous chapters give irregular responses that in some cases resemble quasi-periodic responses and an example is shown in Figure 6.11 (e) for the generalised Hénon map, (5.2):

$$x_{N+1} = a_1 + a_2 x_N + a_3 y_N + a_4 x_N^2 + a_5 x_N y_N + a_6 y_N^2$$

$$y_{N+1} = x_N$$

with a_1 = 0.0, a_2 = -0.4, a_3 = 1.7, a_4 = 1.1, a_5 = -3.3 and a_6 = 0.0; initial values of x and y are given by $x_0 = y_0$ = 0.05. The delay map is given in Figure 6.11 (f) for 5000 iterations. This attractor for 2.5x10^5 iterations is given in Sprott (2003, his Figure 6.1). The attractor is a fractal with fractal dimension 1.368.

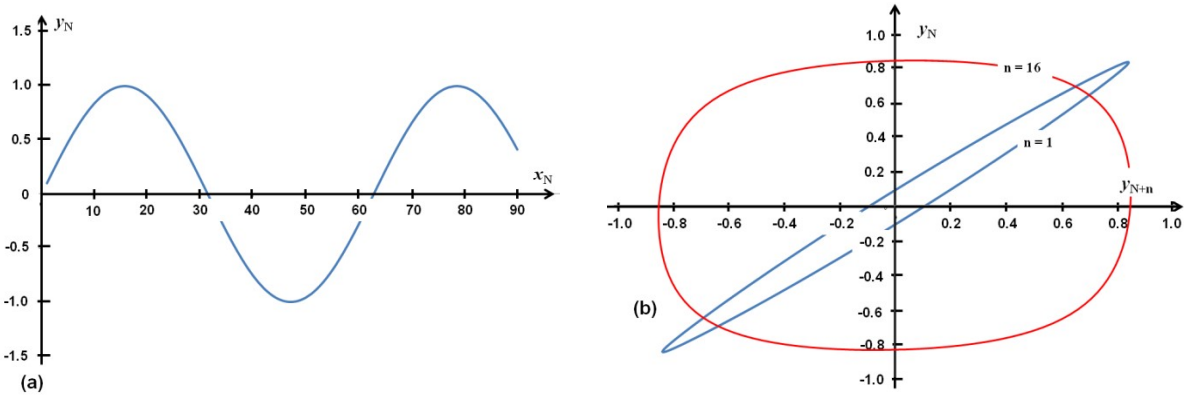

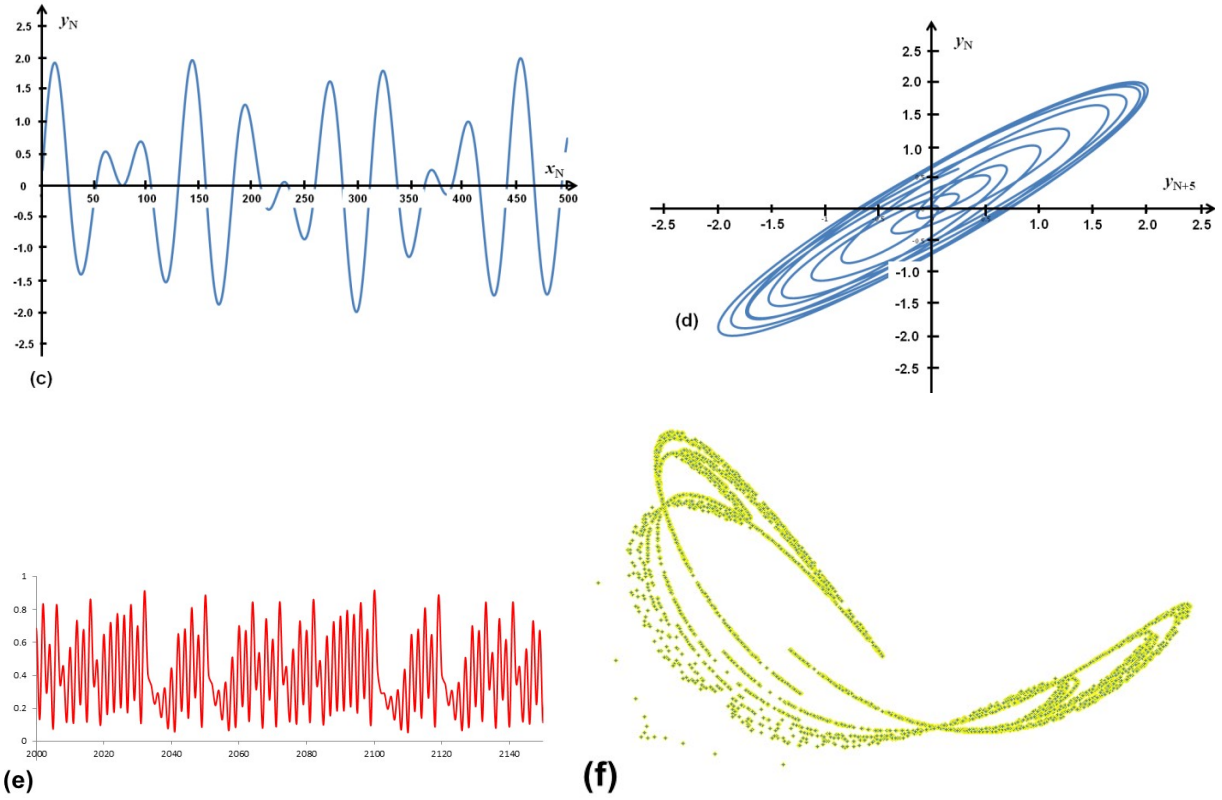

Figure 6.11. Periodic, quasi-periodic and chaotic behaviour with associated delay maps. (a) A periodic signal. (b) Delay maps for a periodic system. If the delay is small, compared to the wavelength, an ellipse results. If the delay is selected to be close to a multiple of the wavelength a map close to a circle results. (c) A quasi-periodic signal given by $y_N = \sin(x_N) + \sin(\sqrt{2}x_N)$. (d) The delay map for the quasi-periodic signal in (c) with a delay of 5. This map consists of nested system of elliptical spirals that never repeat themselves. The figures in both (b) and (d) are attractors but they are not fractals. (e) Response for a generalised Hénon map for 150 iterations. (b) Delay map, produced using EXCEL, for the response in (e) for 5000 iterations. The attractor is a fractal with fractal dimension = 1.368 (see Sprott, 2003, his Figure 6.1).

Another example of a complex fractal geometry is given by Ord (1994). A computer simulation of shear band development in a non-associative plastic material (Figure 6.12 a) was analysed by constructing a delay map (Figure 6.12 c). The velocity of growth of shear bands at a particular value of the shear strain was analysed by recording values of the *x*-component (figure 6.12 a) of the velocity, $(\mathrm{v}_x)_{\mathrm{ij}}$ at a spatial point i, j (after the mean velocity for the deformation is removed) at fixed spatial delays, S, where the value of S ranges from 1 to some larger number (figure 6.12 a, b). Thus a vector, $(\mathrm{v}_x)_{\mathrm{ij}}^{(p)}$, of p dimensions is formed by the array

$$(\mathrm{v}_x)_{\mathrm{ij}}^{(p)} = \left[(\mathrm{v}_x)_{\mathrm{i,j}}, (\mathrm{v}_x)_{\mathrm{i}+S,\mathrm{j}}, \ldots\ldots\ldots\ldots, (\mathrm{v}_x)_{\mathrm{i}+(p-1)S,\mathrm{j}}\right]$$

where the comma in the subscript is there for clarity. Other vectors are then constructed for different values of S. The final array of vectors defines an attractor in p-space. The attractor in 3-space for this model is shown in figure 6.12 (c). Calculations were performed to establish the *embedding dimension* for this attractor; the embedding dimension is that dimension for which the calculated fractal dimension no longer increases. It was established that the embedding

dimension for this attractor is between 4 and 5. Figure 6.12 (c), which is a three dimensional projection of the attractor in 5-space, is a *strange attractor* with a fractal dimension of 2.3.

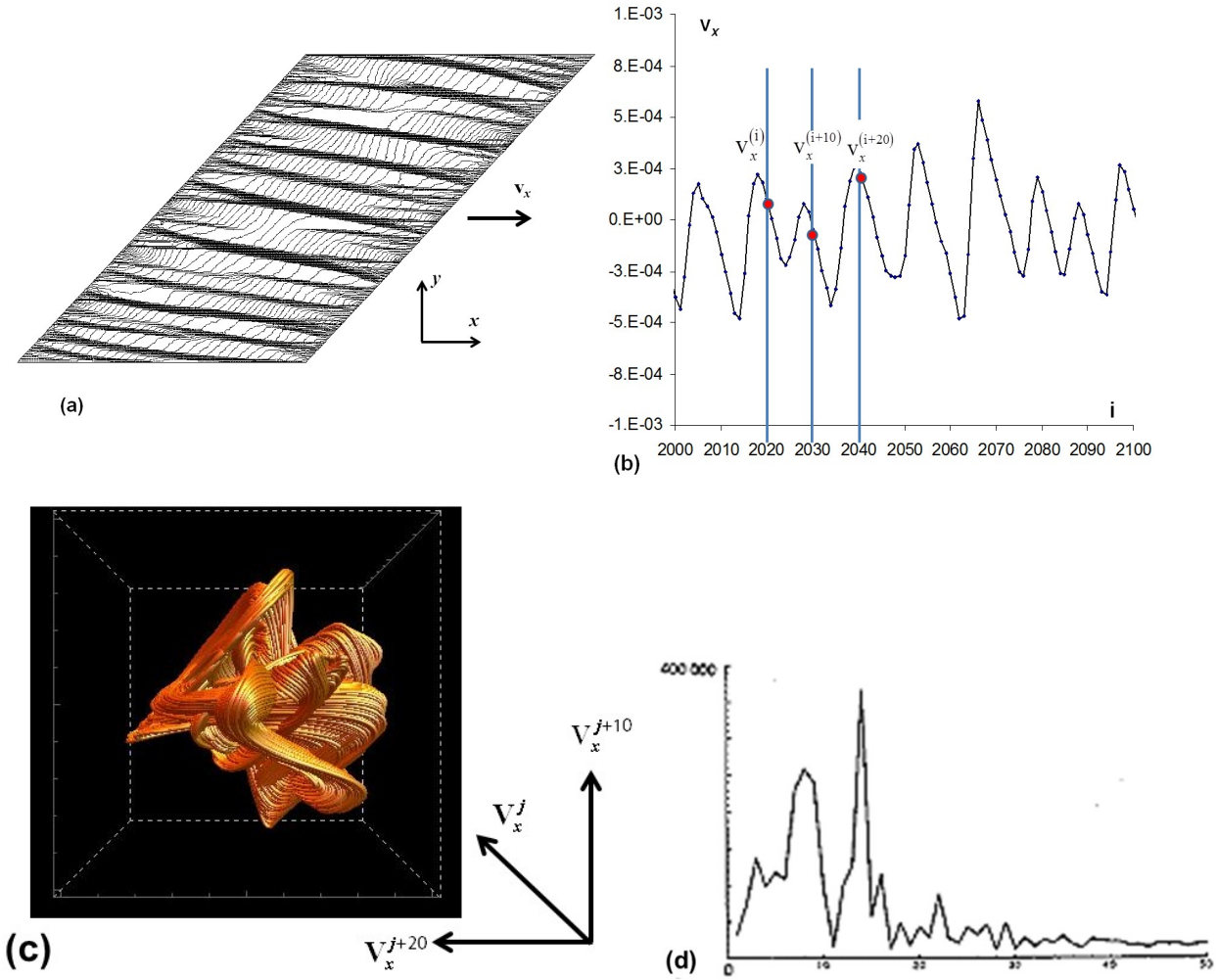

Figure 6.12. An example of a strange attractor derived from delay maps. (a) Plot of *x*-velocity contours in a computer simulation of simple shearing of a Mohr-Coulomb material showing the development of localised zones of shearing. (b) Part of an *x*-velocity profile across the simulation showing the meaning of $v_x^{(i)}$, $v_x^{(i+10)}$ and $v_x^{(i+20)}$ (c) A three dimensional plot of $v_x^{(i)}$, $v_x^{(i+10)}$ and $v_x^{(i+20)}$. This is a three dimensional section through an attractor that exists in 5-space. (d) A Fourier transform of the signal that gives (c).

The construction of delay maps is a fundamental tool in the analysis of chaotic signals and we return to further examples from hydrothermal systems in Chapter 9. Another technique involves establishing the geometry of multifractal systems. Although box counting procedures can be used to explore multifractal geometries, the process is quite cumbersome and can produce erroneous results especially if the singularity measure varies significantly within box sizes greater than a given value (see Arneodo et al., 1987, 1995). We require a fast, compact and quantitative characterisation of seemingly complex data sets that is readily applicable to 1, 2 and 3 dimensional situations and so we turn to a *wavelet* based system that is discussed in detail in Chapter 9. The wavelet approach has many advantages over box counting procedures although a wavelet is basically a "generalised box". Methods of multifractal analysis based on the wavelet transform are particularly applicable to self-similar, intermittent data sets where the wavelet acts as a "microscope" that can zoom into the details of the signal and define local structure and

singularities. Wavelet based software now exists that makes fractal and multifractal analysis fast and efficient so that complex data sets can be completely analysed within minutes using a laptop computer. In addition the wavelet approach is well established within a thermodynamic framework (Bohr and Tel, 1988; Beck and Schlögl, 1993; Arneodo et al., 1995) so that the procedures and results can be placed within a broader mechanics framework.

6.4.2. Some elements of probability theory.

In order to characterise the vast data sets we now have available to us for hydrothermal systems in the form of regional geological, geophysical and geochemical data sets, of mineral compositions and abundances (from hyperspectral data) chemical element abundances (from chemical analyses and XRF-data) and from physical examination (fracture, breccia and vein distributions, alteration intensity) there are a number of techniques commonly used and others not commonly used that are available to us. We refer to these data sets as *signals* and since the signals from hydrothermal systems appear to be stochastic it is natural that probability theory plays a role in their characterisation. We would prefer not simply to use empirical statistical procedures that have no clear grounding in the physical and chemical processes that produced the hydrothermal system but rather use procedures that have a fundamental basis in the thermodynamics of the processes. This section therefore concentrates on some of these thermodynamic approaches to probability distributions although the true basis in thermodynamics is left to Section 6.5 where we introduce a thermodynamic approach based on the statistical mechanics of chaotic systems.

The signals we examine from hydrothermal systems are almost always what are called in the probability literature, *discrete random signals*, for a quantity, X, as opposed to *continuous random signals.* The term *random* here refers to the stochastic (or apparently stochastic) nature of the signal whereas the term *discrete* means the samples are taken at well-defined intervals (not necessarily regular) rather than continuously as might be the case for a continuous XRF scan. Most of the data sets we have from hydrothermal systems are discrete random signals. The *probability distribution* for X is a list of the probabilities (or frequency of occurrence) associated with a given value of X. This is also called the *probability mass function*. Important in probability theory is the concept of an *expected value*, $E(X)$, of X which is *the long term average of a large number of observations*. This is also known as the *mean* or *first moment*. If p_i is the probability of occurrence of x_i then $E(X)$ is given by:

$$E(X) = x_1 p_1 + x_2 p_2 + x_2 p_2 + ...x_k p_k \qquad (6.7)$$

where $p_1 + p_2 + p_2 + ...p_k = 1$

(a) Probability distributions.

The simplest way of characterising a data set is to establish the probability distribution for the data set. We have seen in Chapter 5 that this procedure immediately gives us some insight into the system by establishing whether the distribution has a “light” or “heavy” tail; light tailed distributions are typical of clustered data sets with short range correlations whereas heavy tailed distributions are typical of fractal signals with no characteristic length scale and long range correlations.

Two important parameters that are associated with many probability distributions are the *mean*, μ, and the *standard deviation*, σ (Figure 6.13 a); the *variance* is the square of the standard deviation, σ^2.

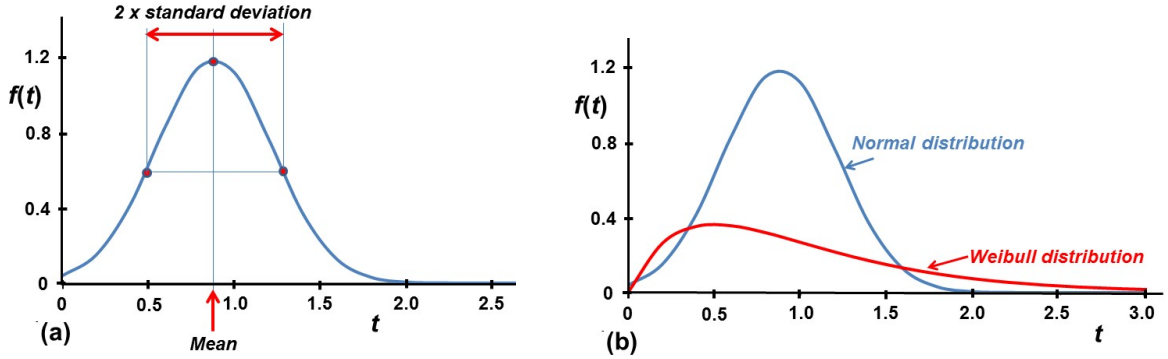

Figure 6.13. Some characteristics of probability distributions. (a) A normal distribution with mean and standard deviation indicated. (b) A normal distribution (blue) and a Weibull distribution (red) with identical values of the mean and variance. The normal distribution is given by $f(t)=\frac{1}{0.3373\sqrt{2\pi}}\exp\left[-\frac{(t-0.88623)^2}{0.22754}\right]$ whilst the Weibull distribution is given by $f(t)=2t\exp\left[-t^2\right]$. The mean in both cases is 0.88623 whilst the variance is 0.11377.

If x_k are the values of a discrete random variable, X, with distribution f(t), where t is a variable of interest, and p_k is the probability of occurrence of x_k then the *mean*, μ_X is defined as

$$\mu_X=\sum_k x_k p_k \qquad (6.8)$$

If the probabilities are equal and k takes the values 1 to n, then, since $\sum_{k=1}^{n} p_k=1$, and $p_1=p_2=\ldots=p_n$,

$$\mu_X=\frac{x_1+x_2+\ldots.x_n}{n}.$$

The *variance*, is defined as

$$\sigma_X^2=\sum_k x_k^2 p_k \qquad (6.9)$$

The *standard deviation*, σ_X, is clearly the square root of the variance.

(b) Moments of a probability distribution.

If we are given only the mean and the standard deviation of a distribution then the distribution is not uniquely defined. An example is shown in Figure 6.13 (b) where a normal distribution and a Weibull distribution are shown with identical mean and standard deviation. In general we need more information than just the mean and standard deviation. This extra information is supplied in the form of *higher moments* of the distribution. The moments (Grinstead and Snell, 1997) of a probability distribution are commonly distinguished as either *raw moments* (also known as *moments about the origin*) or *central moments* (also known as *moments about the mean*). These concepts are illustrated in Figure 6.14.

The raw moments of X are

μ'_k = k^{th} moment of X

$$= \mathrm{E}(X^k)$$
$$= \sum_{j=1}^{\infty} \left(x_j\right)^k p\left(x_j\right) \qquad (6.10)$$

The mean, μ, is known as the *first central moment* of a distribution whereas the variance, σ^2, is known as the *second central moment*; these are given by

$$\mu = \mu_1$$
$$\sigma^2 = \mu_2 - p_1^2$$

The central moments of X are given by

$$\mu_k = \sum_{j=1}^{\infty} \left(x_j - \mu\right)^k p\left(x_j\right)$$

Notice that there exist an infinite number of moments of which the mean and the variance are but two. Moments are particularly important where one needs to manipulate multiple distribution functions. For instance it is commonly difficult to add two or more distribution functions but such exercises are made relatively simple by manipulation of the moments of each distribution (see Grinstead and Snell, 1997, their Chapter 10).

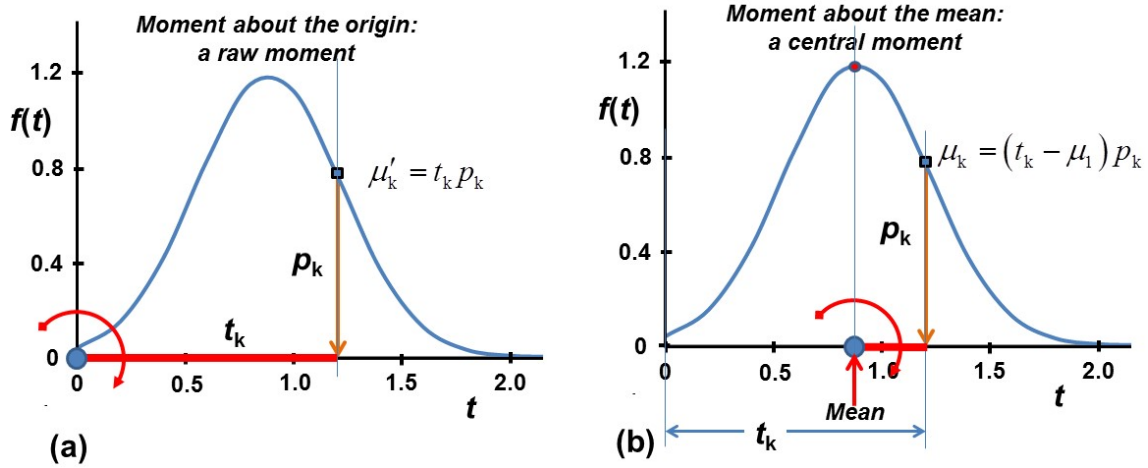

Figure 6.14. An illustration of what is meant by *raw* and *central* moments. One imagines the value of the distribution at the ordinate, t_k, to be equivalent to a weight acting on a lever arm creating a moment about an axis normal to the plane of the page. (a) The lever arm has length, t_k, and the axis is at the origin. This is known as a *moment about the origin* or a *raw moment*, of magnitude, $\mu'_k = t_k p_k$. (b) The lever arm has length, $(t_k - \mu_1)$, where μ_1 is the mean, and the axis is at the mean on the ordinate axis. This is known as a *moment about the mean* or a *central moment*, of magnitude, $\mu_k = (t_k - \mu_1) p_k$. Both of these moments are first moments. A second moment is obtained by squaring the length of the lever arm and so on to higher moments.

(c) Moment generation functions.

Since the moments of probability distributions are so important it is useful to have a way of generating the (in principle infinite) array of moments associated with a particular distribution. Such functions are called *moment generating functions* and are a subset of a much broader group of functions called simply *generating functions*. A generating function for $f(t)$ is of the form:

$$f(t) = a_0 + a_1 t + a_2 t^2 + a_3 t^3 + a_4 t^4 + \ldots . \qquad (6.11)$$

where the a_i's are coefficients to be determined. An apt description of a generating function is that by Wilf (1994): *A generating function is a clothesline on which we hang up a sequence of numbers for display*. The development of the subject depends on the Maclaurin series expansion of a function which is written:

$$f(t) = f(0) + \frac{t}{1!}\frac{\partial f}{\partial t} + \frac{t^2}{2!}\frac{\partial^2 f}{\partial t^2} + \frac{t^3}{3!}\frac{\partial^3 f}{\partial t^3} + \frac{t^4}{4!}\frac{\partial^4 f}{\partial t^4} + \ldots\ldots\ldots + \frac{t^n}{n!}\frac{\partial^n f}{\partial t^n} + \ldots\ldots\ldots$$

This is more conveniently written:

$$f(t) = f(0) + \frac{t}{1!}f^{(1)}(0) + \frac{t^2}{2!}f^{(2)}(0) + \frac{t^3}{3!}f^{(3)}(0) + \frac{t^4}{4!}f^{(4)}(0) + \ldots\ldots\ldots + \frac{t^n}{n!}f^{(n)}(0) + \ldots\ldots\ldots$$

where $f^{(n)}$ is shorthand for the n^{th} derivative, $\frac{\partial^n f}{\partial t^n}$. Thus the a_k in (6.11) can be written: $a_k = \frac{f^{(k)}}{k!} = \frac{1}{k!}\frac{\partial^k f}{\partial t^k}$. Maclaurin series are discussed by Bronsshtein et al. (2003, p 416) who also include an extensive table of Maclaurin series expansions (pp 1009 -1013) for a number of functions. As an example, the Maclaurin series expansion for $f(t) = \exp(\alpha t)$ is

$$f(t) = \exp(\alpha t) = 1 + \frac{\alpha t}{1!} + \frac{\alpha^2 t^2}{2!} + \frac{\alpha^3 t^3}{3!} + \frac{\alpha^4 t^4}{4!} + \ldots\ldots\ldots + \frac{\alpha^n t^n}{n!} + \ldots\ldots$$

The moment generating function of a random variable, X, is defined by

$$M_X(t) = E\exp(tX) \qquad (6.12)$$

where E is the expectation of the distribution and assumes that E exists near to the origin. For a discrete X, (6.12) can be rewritten

$$M_X(t) = \sum_x \exp(tx)P$$

Thus,

$$\begin{aligned} M_X(t) &= \sum_x \exp(tx)f(x) \\ &= \sum_x \left[1 + \frac{xt}{1!} + \frac{x^2t^2}{2!} + \frac{x^3t^3}{3!} + \frac{x^4t^4}{4!} + \ldots\ldots\ldots + \frac{x^rt^r}{r!} + \ldots\ldots\right] f(x) \\ &= \sum_x f(x) + t\sum_x xf(x) + \frac{t^2}{2!}\sum_x x^2 f(x) + \frac{t^3}{3!}\sum_x x^3 f(x) + \ldots\ldots\ldots + \frac{t^r}{r!}\sum_x x^r f(x) + \ldots \\ &= \left[1 + \mu t + \frac{t^2}{2!}\mu_2' + \frac{t^3}{3!}\mu_3' + \frac{t^4}{4!}\mu_4' + \ldots\ldots\ldots + \frac{t^r}{r!}\mu_r' + \ldots\ldots\right] \end{aligned} \qquad (6.13)$$

where μ_r' is the r^{th} moment about the origin of the random variable, X. (6.13) may be used to calculate the raw moments of any distribution where the expected value, E, exists. As an example the raw moments for the normal distribution are:

First raw moment: $E(X) = \mu$

Second raw moment: $E(X^2) = \mu^2 + \sigma^2$

Third raw moment: $E(X^3) = \mu^2 + 3\sigma^2\mu$

Fourth raw moment: $E(X^4) = \mu^4 + 6\sigma^2\mu^2 + 3\sigma^2$

(d) Probability generating functions.

The generating function for a probability distribution of a discrete random variable, *X*, is

$$P(t) = E\left(t^N\right) = \sum_{n=0}^{\infty} f(n) t^n$$

where $f(n)$ is the probability mass function of N and is given by

$$f(k) = \frac{P^{(k)}(0)}{k!}$$

where $P^{(k)}(0)$ is the value of $\frac{\partial^k P}{\partial t^k}$ at $t = 0$. The generating function encodes all of the information contained in the probability distribution.

(e) Probability distribution for a monofractal.

A monofractal has a mass probability distribution (for a discrete data set) given by

$$p(x) = L(x) x^{-\alpha} \quad \text{for } x > x_{min}$$

where $\alpha > 1$ (otherwise the area under the curve is infinite) and $L(x)$ is a slowly varying function. For the most part $L(x)$ is a constant. In general the probability function can be written

$$p(x) = \frac{\alpha - 1}{x_{\min}} \left(\frac{x}{x_{\min}} \right) x^{-\alpha}$$

The moments of this distribution are given by

$$\left\langle x^m \right\rangle = \frac{\alpha - 1}{\alpha - 1 - m} x_{min}^m$$

Thus when $\alpha < 2$, the average and all higher order moments are infinite; when $2 < \alpha < 3$ the mean exists but the variance and all higher order moments are infinite. Thus power law distributions have a well-defined mean only if $\alpha > 2$ and have a finite variance only if $\alpha > 3$. Thus it is incorrect to apply methods commonly used in classical statistics (such as regression) that are based on the concept of *standard deviation* to many power-law distributions. It is somewhat curious that most of the phenomena we encounter in hydrothermal systems are not capable of being rigorously analysed using classical probability theory (see Zaliapin et al., 2005) although such methods are in widespread use.

In many instances, because the system involved is of finite size the distribution follows a power law up to a certain size and then shows an exponential cut-off (see Figure 6.6 (f) for instance):

$$p(x) = L(x) x^{-\alpha} \exp(-\lambda x)$$

Such *finite size effects* are common in critical systems.

(f) Probability distribution for a multifractal.

Mandelbrot (2003) draws the distinction between the *Fourier analysis* of a function and the *"Holder analysis"* of a multifractal measure. Whereas a Fourier analysis decomposes a

function into a sum of components each of which is characterised by a fixed frequency (Figures 6.9 b, d), a Holder analysis decomposes a measure into a continuous sum of measures each characterised by a value of the Holder exponent, α. Each α measures the strength of a local singularity (or "roughness") and exists on a set of fractal dimensions, $f(\alpha)$. In order to establish the singularity spectrum for a multifractal one starts by covering the fractal with boxes of size L on edge in exactly the same way as for box counting a mono-fractal. The probability measure of the i^{th} box is $P_i \propto L^{\alpha_i}$ which defines the *singularity index*, α_i; this is also called the *Lipshitz-Holder exponent*:

$$\alpha_i = \frac{\ln P_i}{\ln L} \qquad (6.14)$$

One then counts the number of boxes, $\mathcal{N}_\alpha$, for which α_i is between α and $\alpha + \mathrm{d}\alpha$. This number, for a large number of boxes (that is, small L), is proportional to $L^{-f(\alpha)}\mathrm{d}\alpha$. The fractal is represented by an interwoven set of singularities and the quantity, $f(\alpha)$, is the fractal dimension of the set with Lipshitz-Holder exponent, α (Figure 6.15 a, b).

The main constraint on $f(\alpha)$ is that it is $\cap-$shaped as shown in Figure 6.5 where we present an argument for this $\cap-$shape. The following discussion gives some additional feeling for why this $\cap-$shaped distribution exists. Fractals representing high values of a measure (that is, small α) have a low dimension, $f(\alpha)$, meaning that they fill space in a sparse manner although this does not preclude some clustering. Similarly, fractals representing a small measure (that is, large α) also have a small $f(\alpha)$ and hence are also sparsely distributed in space although again clustering is not precluded. On the other hand fractals representing a medium measure have a high $f(\alpha)$ and hence tend to fill space more uniformly. These trends are shown in Figure 6.15.

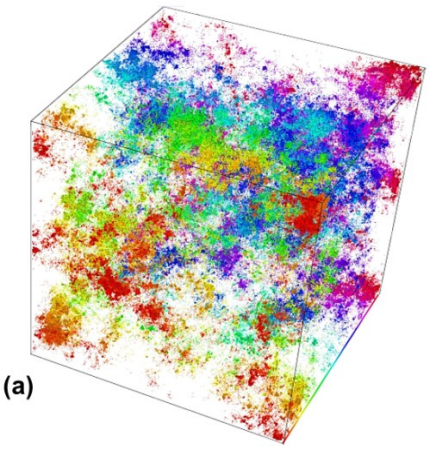

(a)

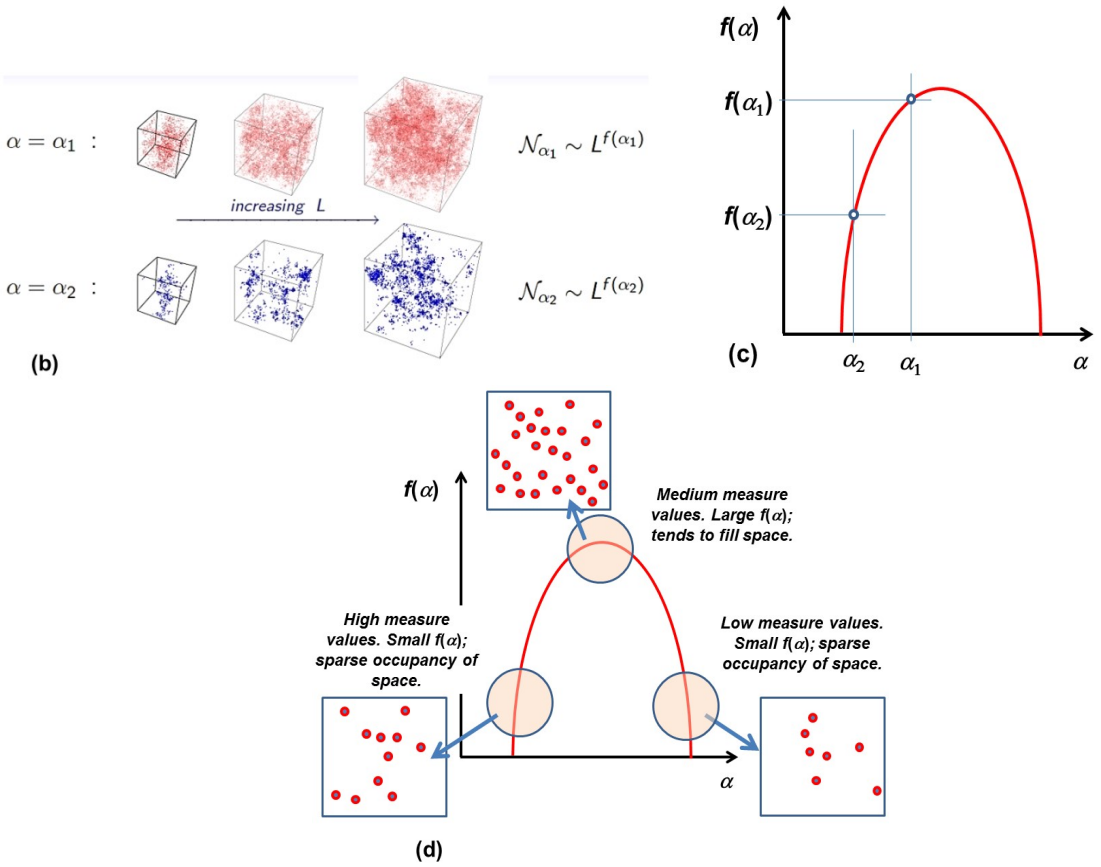

Figure 6.15. A summary of the multifractal concept.The meaning of α and $f(\alpha)$. (a) A multifractal in which the various measures are represented in different colours. This could easily be a representation of gold distribution with each colour representing a different grade. From Ridriguez et al. (2009). (b) Two different fractals are selected from the mutifractal represented by the measure in (a). One has a singularity strength (a direct indication of the logarithm of the measure) of α_1 and the other of α_2. We suppose that $\alpha_1 > \alpha_2$. As one increases the box size, L, for the singularity of strength α_1 the proportion, $\mathcal{N}\alpha_1$, increases as $L^{f(\alpha_1)}$ with a similar statement for α_2 and $\mathcal{N}\alpha_2$. Since the α_1-measure fills space more than the α_2-measure, $f(\alpha_1) > f(\alpha_2)$. Thus the relation shown in (c) results. If one continues this process for all of the α's then the full $\bigcap$−curve shown in (c) results. (d) A summary of the above relations.

(g) Some thermodynamic analogies for multifractals.

With the above discussion in mind let us now explore the multifractal concept in greater detail. As we have indicated, a multifractal consists of groups of fractal objects, each with a different measure, interwoven in space. The resulting geometry may or may not appear self-similar depending on the complexity of the inter-relations between the various fractals. It is common (Fedor, 1988, and see also Figure 6.15 a, b) to represent the range of singularity measures for multifractals by the expression

$$N_\alpha(\varepsilon) = \varepsilon^{-f(\alpha)} \qquad (6.15)$$

which is a generalisation of (6.1) so that D in (6.1) is replaced by a spectrum, $f(\alpha)$, of singularity measures. α is commonly known as the *Holder exponent* and is also known as the Lipshitz exponent. The function $f(\alpha)$ appears as a $\cap$–shaped curve represented by a plot of $f(\alpha)$ against α as shown in Figure 6.16 (a). The reason for this particular shape relies on arguments in statistical mechanics which we explore below in Section 6.5 but in anticipation of that discussion we note that from a thermodynamic point of view the singularity spectrum is equivalent to an entropy function. In classical thermodynamics the entropy, S, of a system as a function of energy is a $\cap$–shaped curve (Callen Chapter 4) as shown in Figure 6.16 (b) which is also that of a multifractal distribution.

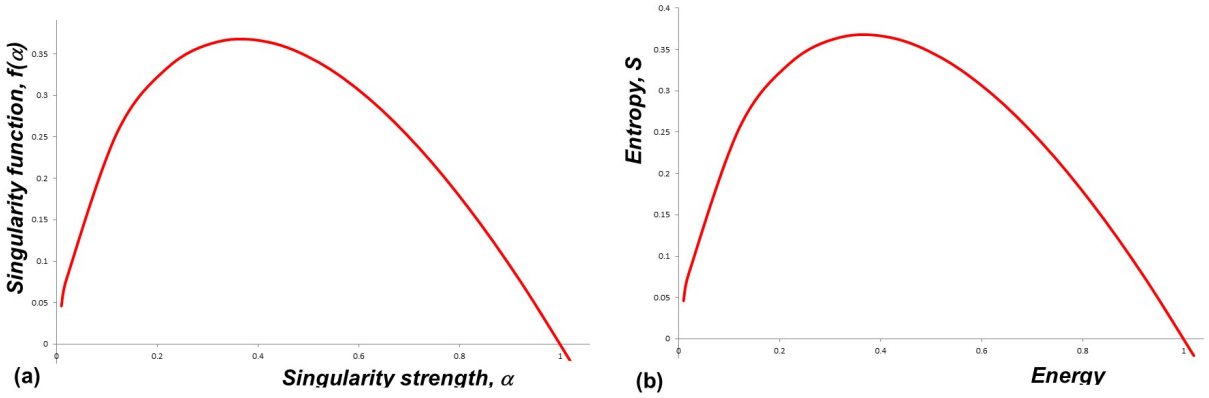

Figure 6.16. The correspondence between the thermodynamic entropy and the multifractal singularity spectrum. (a) A plot of the multifractal singularity function, $f(\alpha)$ against the strength of the singularity, α. (b) A plot of entropy, S, against the energy of the states existing in the system.

In general the spectrum of singularity measures needs to be established by direct measurement but it is important in the interpretation of these spectra to be able to make comparisons with spectra generated by specific models. Some examples are shown in Table 6.3 adapted largely from Halsey et al. (1986) and from Arneodo et al. (1989). In the table, D_0 is the value of $[f(\alpha)]^{max}$ and D_∞, $D_{-\infty}$ are the values of α for $f(\alpha) = 0$. The last row in the table is adapted from Arneodo et al. (1995).

Table 6.3. Singularity spectra resulting from various models.

Recursive Model	Result	Singularity Spectrum
Power-law probability distribution $p(x) = \tilde{a}x^{\tilde{a}-1}$	Bifractal. Fractal states at (0,0) and (1,1)	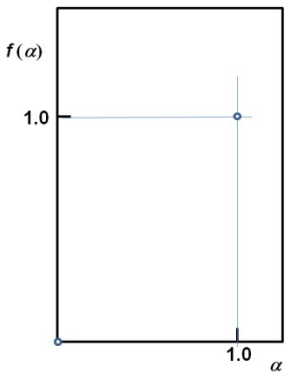

Uniform Cantor set. $p_1 = p_2 = p_3 = \frac{1}{2}$ $l_1 = l_2 = l_3 = \frac{1}{3}$	Monofractal. Fractal state at $\left[\frac{\ln 2}{\ln 3}, \frac{\ln 2}{\ln 3}\right]$	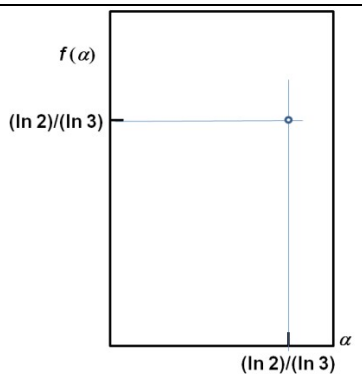
Two-scale Cantor set. $p_1 = \frac{3}{5}, p_2 = \frac{2}{5}$ $l_1 = \frac{1}{4}, l_2 = \frac{2}{5}$	Multifractal.	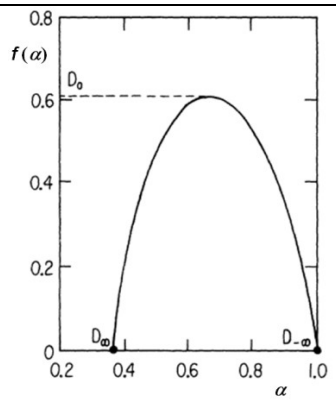
Generalised Cantor set – I. $p_1 + 2p_2 = 1$ $l_1 + 2l_2 = 1$ $p_2/l_2 > p_1/l_1$ $l_2 > l_1$	Incomplete multifractal.	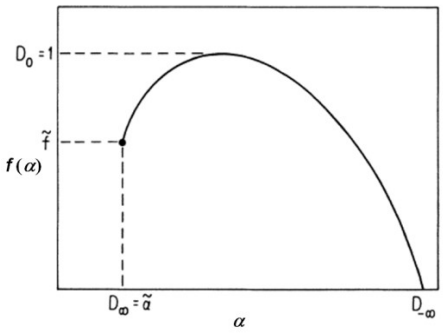
Generalised Cantor set - II. $p_1 = p_3 \neq p_2$ $l_1 = l_3 \neq l_2$	Bifractal. $\tilde{f} = \frac{\ln\left(\frac{1}{2}\right)}{\ln l_2}, \tilde{f} = \frac{\ln\left(\frac{1}{2}\right)}{\ln l_2},$	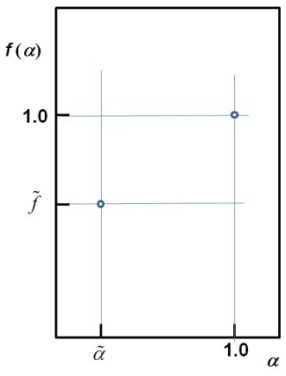

Period doubling cascade. $x_{n+1} = \lambda\left(1-2x^2\right)$	Multifractal.	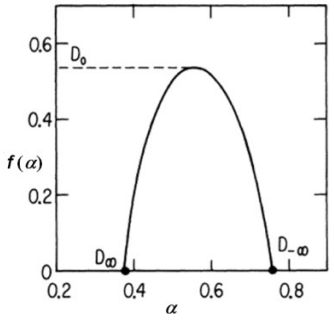
Mode locking cascade.	Multifractal.	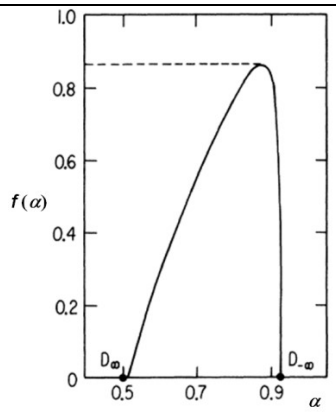
Quasi-periodic circle map.	Multifractal.	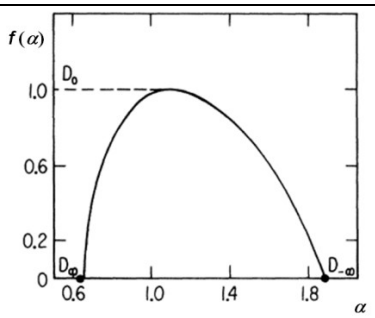
Multifractal Devil's staircase with superimposed sine wave.	Multifractal with phase change: singular to non-singular (Arneodo et al., 1993).	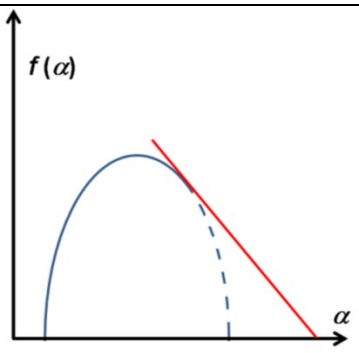

(h) Generalised fractal dimensions.

At times other quantities are used instead of $f(\alpha)$. This is the set of *generalised fractal dimensions*, D_q; the $f(\alpha)$ and the D_q are related by:

$$D_q = \frac{1}{q-1}\left[q\alpha - f(\alpha)\right]$$

where $q = \frac{\mathrm{d}f(\alpha)}{\mathrm{d}\alpha}$

We also have $\alpha = \frac{\mathrm{d}}{\mathrm{d}q}\left[(q-1)\mathrm{D}_q\right]$

and $f(\alpha) = q\frac{\mathrm{d}}{\mathrm{d}q}\left[(q-1)\mathrm{D}_q\right] - (q-1)\mathrm{D}_q$

The generalised fractal dimension, D_q, is also related to the scaling exponent for the q^{th} moment of the measure μ. If we have a set of measures, say the concentration of a chemical component such as gold distributed over a fabric, we define the partition function, $\mathbb{Z}(q,\varepsilon)$, in terms of the q^{th} moment of the distribution for μ and for a box size ε as (Lynch, 2007):

$$\mathbb{Z}(q,\varepsilon) = \sum_{i=1}^{N(\varepsilon)} \mu_i^q(\varepsilon) \tag{6.16}$$

Then we can also define $\tau(q)$ as

$$\tau(q) = \lim_{\varepsilon\to 0}\frac{\ln\mathbb{Z}(q,\varepsilon)}{-\ln\varepsilon} \tag{6.17}$$

The generalised fractal dimensions D_q are given by:

$$\tau(q) = D_q(1-q) \tag{6.18}$$

In the limit $\varepsilon \to 0^+$, $\mathbb{Z}(q, \varepsilon)$ behaves as a power law:

$$\mathbb{Z}(q,\varepsilon) \approx \varepsilon^{-\tau(q)} \tag{6.19}$$

The relations between the $f(\alpha)$ singularity spectrum, q and the $\tau(q) = (1-q)D_q$ spectrum are given (Arneodo et al., 1995) by:

$$q = \frac{\mathrm{d}f(\alpha)}{\mathrm{d}\alpha}$$

$$\frac{\mathrm{d}^2 f(\alpha)}{\mathrm{d}\alpha^2} < 0$$

$$\tau(q) = q\alpha - f(\alpha) \tag{6.20}$$

These relations are illustrated in Figure 6.17 (a).

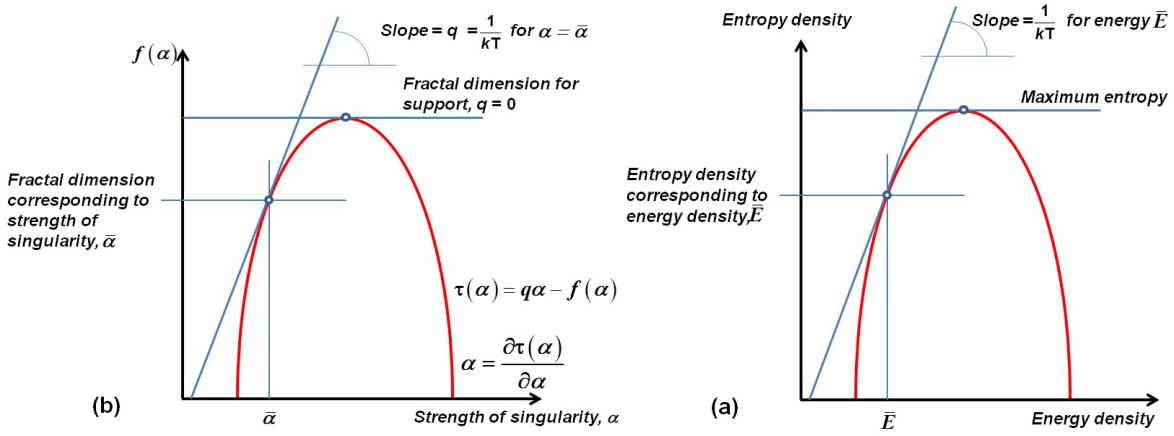

Figure 6.17. Some features of the singularity spectrum. (a) τ as the Legendre Transform of $f(\alpha)$: $\tau(q)=\frac{\mathrm{d}f(\alpha)}{\mathrm{d}\alpha}\alpha - f(\alpha), q=\frac{\mathrm{d}f(\alpha)}{\mathrm{d}\alpha}=0$ corresponds to the tangent at $[f(\alpha)]^{max}$. (b) The thermodynamic interpretation of the singularity spectrum. $f(\alpha)$ corresponds to the entropy per unit volume whilst α corresponds to the energy per unit volume. $[f(\alpha)]^{max}$ corresponds to the maximum entropy per unit volume whilst the slope of the tangent to the singularity spectrum corresponds to the Boltzmann temperature $\mathbb{B}$ (see Bohr and Tel, 1988; Arneodo et al., 1995).

There are strong analogies with thermodynamic functions and there is a basis in statistical mechanics for interpreting these functions from a thermodynamic point of view (Bohr and Tel, 1988; Arneodo et al., 1995). We elaborate on such concepts in Section 6.5 but as a summary: The function $f(\alpha)$ is identified with the entropy per unit volume, α_i with the energy, E_i, per unit volume of a microstate, i, q with the Boltzmann temperature, $\mathbb{B}=\frac{1}{k\mathrm{T}}$, and the $\tau(q)$ spectrum is the Legendre transform (see Callen, 1985, his Chapter 5; Hobbs and Ord, 2015, pp 134-135) of the $f(\alpha)$ spectrum. $\mathbb{Z}$ can be written

$$\mathbb{Z}(\mathbb{B})=\sum_i \exp(-\mathbb{B}E_i) \qquad (6.21)$$

Some of these interpretations are illustrated in Figure 6.17 (b). This thermodynamic interpretation of fractals and particularly of multifractals is explored by Bohr and Tel (1988), Beck and Schlögl (1993) and by Arneodo et al. (1995, 2003) who point out that such thermodynamic properties of multifractals place limitations on the characterisation of multifractals by the box counting procedure and why a resort to wavelet analysis is a better approach. Notice that for q = 0, 1, 2, D_q corresponds to well-known functions. Thus D_0 is the *box dimension* for the support of the multifractal and is equivalent to D in (6.1), D_1 is the *information dimension* (6.3) and D_2 is the *correlation dimension* (6.4). These dimensions, together with D_∞ and $D_{-\infty}$ illustrated in Table 6.3 are useful in comparing different singularity spectra.

6.5. A short discussion of statistical mechanics: The relation between classical thermodynamics and the multifractal formalism.

The multifractal concept is not only a convenient way of thinking about fractals embedded in other fractals and that scale in different ways according to the local length scale, the concept is deeply grounded in thermodynamics. This is one reason why the concept is appealing since it is not an arbitrary statistical concept but has a strong basis in the physics and chemistry

of nonlinear dynamical systems (Beck and Schlögl, 1993). Here we give a brief discussion of the close connection between classical thermodynamics and statistical mechanics as developed by Boltzmann and Gibbs and the multifractal formalism. Both concepts are based on the fact that the systems of interest (chemical systems in general, and nonlinear dynamical systems in particular) comprise *a large number of parts* (*molecules* on one hand and *chaotic states* on the other) and that the macroscopic behaviour of such systems can be treated in terms of *probabilities*. *Statistical Mechanics* is a formalism for establishing physical interpretations of thermodynamic quantities such as temperature, pressure, internal energy, entropy, Gibbs energy and Helmholtz energy in terms of the probability distributions of the energies of microstates. Identical quantities can be defined for nonlinear dynamical systems in the *thermodynamics of chaotic systems* in terms of the probability distributions of chaotic states of the system (Beck and Schlögl, 1993).

Most textbooks on classical thermodynamics present the *first and second laws of thermodynamics* as axioms that have a basis in day to day experience. Associated with these laws are the concepts of *internal energy* and *entropy* that are similarly presented as functions that need no definition. As an example of such an axiomatic approach one should consult the first edition of the classical work by Callen (1960).

However (see the second edition of Callen, 1985, or Atkins, 1978, Chapter 20) the laws of thermodynamics and functions such as the internal energy, and entropy can be derived simply by considering the behaviour of such systems as resulting from the result of averaging the motions of a large number of molecules. The operative phrase here is *a large number* and the subject known as *thermodynamics* can be thought of as a group of relations that describes the most probable macroscopic behaviour of a large number of moving particles (molecules). In an identical manner, conceptually, the multifractal formalism can be thought of as one relation that describes the behaviour of a large number of micro-states that arise from the collective interactions of processes operating in the system (Beck and Schlögl, 1993).

The subject that is concerned with the macroscopic behaviour of a large number of elements of a system is called *statistical mechanics* and is pertinent to any physical or chemical system that is comprised of a large number of parts. The subject is based on considering the probability, $P(E_i)$, that a system in contact with a large heat reservoir[3] is in a state with energy, E_i, and supposes that this probability is proportional to the number of ways in which the reservoir can adjust itself to accommodate the remainder of the energy, $(E_{total} - E_i)$, where E_{total} is the energy of the reservoir plus that of the system.

If this accommodation can occur in $\mathbb{W}$ different ways, where $\mathbb{W}$ is a function of $(E_{total} - E_i)$, then

$$P(E_i) = C\mathbb{W}$$

where C is a constant. The procedure is to expand $\ln\mathbb{W}$ as a Taylor series. The logarithm is taken since the logarithm changes more slowly than the energies. Thus,

[3] Atkins (1978, p645) points out that the reservoir need not be distinct from the system under consideration but can be the system itself so long as it is large.

$$\ln\mathbb{W} = \ln\mathbb{W}\left(E_{total}\right) - \left(\frac{\partial \ln \mathbb{W}}{\partial E}\right)_{E_{total}} E_i + \textit{terms involving higher powers of } E_i$$

Since E_i is small compared to E_{total}, and $\left(\frac{\partial \ln \mathbb{W}}{\partial E}\right)_{E_{total}}$ is a constant (that we will call β) that depends only on E_{total} we can write

$$\ln\mathbb{W} = \ln\mathbb{W}\left(E_{total}\right) - \beta E_i$$

Thus,

$$\mathbb{W} = \mathbb{W}\left(E_{total}\right)\exp\left(-\beta E_i\right)$$

So that,

$$P\left(E_i\right) = C\mathbb{W}\left(E_{total}\right)\exp\left(-\beta E_i\right)$$

The quantity $\mathbb{W}\left(E_{total}\right)$ is a property of the reservoir and is independent of the state of the system and so can be combined with C to give a new constant, C', such that the sum of all the probabilities is one:

$$\sum_i P\left(E_i\right) = C'\sum_i \exp\left(-\beta E_i\right)$$

so that

$$C' = \frac{1}{\sum_i \exp\left(-\beta E_i\right)}$$

and so

$$P\left(E_i\right) = \frac{\exp\left(-\beta E_i\right)}{\sum_i \exp\left(-\beta E_i\right)} \qquad (6.22)$$

This is the fundamental result of statistical mechanics and is known as the *canonical distribution.* From this one can define the *internal energy* of the system as

$$\langle E\rangle = \sum_i E_i\, P\left(E_i\right) = \frac{\sum_i E_i \exp\left(-\beta E_i\right)}{\sum_i \exp\left(-\beta E_i\right)} \qquad (6.23)$$

The sum of $\exp\left(-\beta E_i\right)$ over all of the energy states in the system occupies a central role in statistical mechanics and is called the *canonical partition function*, $\mathbb{Z}$:

$$\mathbb{Z} = \sum_i \exp\left(-\beta E_i\right) \qquad (6.24)$$

which is equivalent to (6.21). In addition, all the classical thermodynamic state variables and functions can be derived from (6.22). One should consult Sornette (2006) and (Beck and Schlögl, 1993) for a detailed discussion of these subjects. A comparison of the classical thermodynamic and multifractal quantities is given in Table 6.3.

Table 6.3. Comparison of classical thermodynamic multifractal quantities.

Classical Thermodynamics	Thermodynamics of multifractals
$\beta = \frac{1}{T}$	q

β is the reciprocal of the temperature, T.	$q = \frac{df(\alpha)}{d\alpha}$ q is the slope of the tangent to the singularity spectrum
Energy	α Singularity strength Conjugate of q
G = U - TS Gibbs energy Legendre transform of Helmholtz energy	$\tau(q) = q\alpha - f(\alpha)$ $= (q - 1)/D_q$ Legendre transform of $f(\alpha)$
S Entropy	$f(\alpha)$ Conjugate of τ(q)
$\mathbb{Z}(\beta)$ Thermodynamic partition function	$\mathbb{Z}(q)$ Multifractal partition function
$\psi = -\ln\mathbb{Z}(\beta)$ Helmholtz energy	$\psi = -\ln\mathbb{Z}(q)$ Statistical Helmholtz energy